Notch-Induced miR-708 Antagonizes Satellite Cell Migration and Maintains Quiescence

Meryem Baghdadi, Joao Firmino, Kartik Soni, Brendan Evano, Daniela Di Girolamo, Philippos Mourikis, David Castel, Shahragim Tajbakhsh

Notch induced mir-708 antagonizes satellite cell migration and maintains quiescence

Meryem B. Baghdadi[1,2,3], Joao Firmino[4], Kartik Soni[1,2], Brendan Evano[1,2], Daniela Di Girolamo[5], Philippos Mourikis[6], David Castel[7,8], Shahragim Tajbakhsh[1,2 *#].

1: Stem Cells and Development, Department of Developmental & Stem Cell Biology, Institut Pasteur, Paris 75015, France.
2: CNRS UMR 3738, Institut Pasteur, Paris 75015, France.
3: Sorbonne Universités, UPMC, University of Paris 06, IFD-ED 515, 4 Place Jussieu, Paris 75252, France.
4: Bioimaging and Optics platform (BIOP), School of Life Sciences, Swiss Federal Institute of Technology (EPFL), Lausanne, Switzerland.
5: Dipartimento di Medicina Clinica e Chirurgica, Università degli Studi di Napoli Frederico II, Via S. Pansini 5, 80131, Naples, Italy.
6: INSERM IMRB U955-E10, UPEC, ENVA, EFS, Créteil 94000, France.
7: UMR8203 "Vectorologie et Thérapeutiques Anticancéreuses", CNRS, Gustave Roussy, Univ. Paris- Sud, Université Paris-Saclay, 94805, Villejuif, France.
8: Département de Cancérologie de l'Enfant et de l'Adolescent, Gustave Roussy, Univ. Paris-Sud, Université Paris-Saclay, 94805, Villejuif, France.

[#] Lead contact
*Correspondence: shahragim.tajbakhsh@pasteur.fr

Key words: Skeletal muscle stem cell, satellite cell, microRNA, quiescence, niche, migration, tensin3, focal adhesion

SUMMARY

Critical features of stem cells include anchoring within a niche and activation upon injury. Notch signalling maintains skeletal muscle satellite (stem) cell quiescence by inhibiting differentiation and inducing expression of extracellular components of the niche. However, the complete spectrum of how Notch safeguards quiescence is not well understood. Here we perform Notch ChIP-sequencing and small RNA sequencing in satellite cells and identify the Notch-induced microRNA-708, which is a mirtron that is highly expressed in quiescent cells and sharply downregulated in activated cells. We employ *in vivo* and *ex vivo* functional studies, in addition to live imaging, to show that miR-708 regulates quiescence and self-renewal by antagonizing cell migration through targeting the transcripts of the focal adhesion-associated protein, Tensin3. Therefore, this study identifies a Notch-miR708-Tensin3 axis and suggests that Notch signaling can regulate satellite cell quiescence and transition to the activation state through dynamic regulation of the migratory machinery.

INTRODUCTION

The regenerative ability and plasticity of adult skeletal muscle is largely due to its resident muscle satellite cells (Sambasivan and Tajbakhsh, 2015). In resting muscle, satellite cells are quiescent and express the paired-box transcriptional factor *Pax7* (Seale et al., 2000). Following injury, they re-enter the cell cycle, proliferate to generate myoblasts that further differentiate and fuse to restore the damaged fibre, while a subpopulation of myogenic cells returns to quiescence for self-renewal of the satellite cell pool (Baghdadi and Tajbakhsh, 2018).

Notch is a crucial regulator of satellite cells as the specific depletion of RBPJ, the DNA binding factor essential for mediating canonical Notch signalling, leads to spontaneous differentiation that leads to progressive loss of satellite cells (Mourikis et al., 2012b; Bjornson et al., 2012). Notch activity antagonizes myogenesis by induction of transcriptional repressors (members of the HES/HEY family) (Mourikis et al., 2012b; Bjornson et al., 2012) and we recently showed that Notch-induced production of Collagen V by satellite cells is a critical component of the quiescent niche, as its depletion leads to gradual diminution of the stem cell pool (Baghdadi et al., 2018). However, it remains unclear if this pleiotropic signalling pathway maintains stem cells by controlling additional cellular processes other than differentiation and niche composition.

MicroRNAs (miRNAs) are essential for muscle homeostasis and regeneration upon injury as the conditional deletion of *Dicer* (an RNAse III endonuclease required for maturation of miRNAs) in the PAX7+ population, results in a depletion of satellite cells and a quasi-absence of repair upon injury (Cheung et al., 2012). Although numerous miRNAs were reported to regulate myoblast proliferation and differentiation (Kirby et al., 2015), only miR-489 (Cheung et al., 2012) was shown to regulate satellite cell quiescence and/or self-renewal.

We performed RNA-sequencing on primary skeletal muscle cells (Castel et al., 2018) and identified the quiescence specific miR-708 that is regulated by Notch signaling. We show that this micro-RNA plays a critical role in satellite cell maintenance and migration in the niche by targeting *Tensin3* (*Tns3*) mRNA, which encodes a fibrillar adhesion protein that physically links integrins and the actin cytoskeleton (Qian et al., 2009). Therefore, we identify a miR-708 that acts as a gatekeeper of quiescence by modulating muscle stem cell migration.

RESULTS

A quiescence-specific microRNA is regulated by Notch signalling in satellite cells

To identify miRNAs that regulate cellular quiescence, we performed RNA-deep sequencing on freshly isolated satellite cells (QSC), *in vitro* activated satellite cells for 60h (ASC) and differentiated cells cultured for 7 days (DIFF) (Fig. 1A; (Castel et al., 2018)). We found that miR-708 was enriched in quiescent satellite cells (Fig. 1A). Real-time quantitative PCR (RT-qPCR) analysis showed miR-708 expression to be significantly decreased *in vivo* in ASCs 5 days post injury, and in freshly isolated myofibres compared to freshly isolated satellite cells (Fig. S1A). Interestingly, miR-708 is a highly conserved mirtron (Ruby et al., 2007) encoded in the quiescence-specific gene *Odz4*/*Tenm4* (Fig. S1B). As is the case with other mirtrons, miR-708 does not have its own promoter, therefore its expression depends on that of *Odz4*.

Interestingly, *Odz4* expression decreases in Notch-depleted myogenic progenitors in embryos (*Pax3*$^{Cre/+}$*; Rbpj*$^{-/-}$*; Myod*$^{-/-}$)(Brohl et al., 2012) suggesting a potential link with Notch signalling. We confirmed this hypothesis by interrogating genome-wide ChIP-seq data in adult murine myoblasts (Castel et al., 2013). Notably, two NICD and RBPJ binding sites were identified as most proximal to the *Odz4* locus (Fig. 1B). The combination of histone modifications H3K4me1, H3K27ac, and the acetyltransferase p300 (Fig. 1B), in addition to their ability to induce transcription upon Notch activation in cell-based luciferase assays (Fig. 1C), indicates that these sequences are in *bona fide* enhancers.

Using genetically modified mice for Notch ablation (*Tg:Pax7-CT2; Rbpj*^{Flox} (Mourikis et al., 2012b), Fig. 1D and Fig. S1C), or gain-of-function (*Myf5*^{Cre}*;R26*$^{NICD\text{-}nGFP}$(Mourikis et al., 2012a), Fig. 1E and Fig. S1D) we showed that transcription of miR-708 (but not miR-489, another quiescent miRNA (Cheung et al., 2012)) and *Odz4* tightly followed Notch activity. We confirmed their transcriptional responses in satellite cells isolated from *Tg:Pax7-nGFP* postnatal day 8 (P8) pups in which endogenous Notch activity gradually declines as cells transit from an upstream Pax7^{High} to a committed Pax7^{Low} state (Mourikis et al., 2012b; Rocheteau et al., 2012) (Fig. 1F and Fig. S1E). Taken together, these data demonstrate that RBPJ/NICD signalling regulates the expression of *Odz4,* and by consequence miR-708, in satellite cells *in vivo* by direct binding on distal transcriptional enhancers.

miR-708 retains stemness and self-renewal capacities of satellite cells *ex vivo*

To assess whether the sustained expression of miR-708 affects satellite cell behaviour, we transfected freshly isolated satellite cells with a synthetic miR-708 molecule (Mimic-708; Fig. S1F-G for validation, specificity) and scored for proliferation (EdU+) and differentiation (Myogenin+). Interestingly, miR-708 overexpression exhibited a delay in cell cycle entry (24h) and proliferative capacity (48h) (Fig. 1G), and a decrease in the number of MYOG+ cells compared to control at 72h and 4 days (Fig. 1H). Taken together, these results show that miR-708 significantly impedes satellite cell proliferation and differentiation, properties reminiscent of activation of Notch signalling.

In a complementary loss-of-function assay, we depleted miR-708 using short-interfering RNA (AntimiR-708, Fig. S1H) in an *ex vivo* system where resident satellite cells on isolated myofibres exit quiescence, enter the myogenic program and form clusters composed of proliferating ($PAX7^+/MYOD^+/MYOG^-$), differentiated ($PAX7^-/MYOG^+$) and self-renewed ($PAX7^+/MYOG^-$) cells (Zammit et al., 2004). Targeting specifically miR-708-5p increased significantly the number of differentiated cells per fibre, and reduced the number of self-renewed cells (Fig. 1I).

A concern with experiments involving miR-708 manipulations is the putative effect on *Odz4* expression, as germline deletion of this gene results in reduced numbers of myofibres and satellite cells (Ishii et al., 2015). However, no miR-708 binding sites were noted in the 3'UTR of *Odz4*, indicating that it is not a miR-708 target. Furthermore, *Odz4* levels were not altered following miR-708 overexpression (Fig. S1I). Finally, the induction of miR-708 in *Odz4*-deficient primary satellite cells (Fig. S1J) rescued their precocious differentiation phenotype (Fig. 1J). Thus, we conclude that in this context, the anti-myogenic effect of miR-708 was not due to *Odz4* function.

Antagonism of miR-708 in vivo induces spontaneous exit from quiescence and premature differentiation of satellite cells

To investigate the functional role of miR-708 *in vivo*, we synthesized a miR-708 antagonist (AntagomiR-708) with an antisense sequence to mature miR-708-5p, as well as control Scramble. Importantly, RT-qPCR analysis on different cell populations extracted from skeletal muscles, namely endothelial cells, fibro-adipogenic progenitors, resident and infiltrating macrophages revealed that only satellite cells expressed miR-708 (data not shown). We then labelled the majority of satellite cells with a tamoxifen inducible membrane-GFP using *Tg:Pax7-CreERT2; R26^{mTmG}* lineage-

traced mice (~95% recombination efficiency, Fig. S2A). Surprisingly, 10 days after injection (Fig. 2A), isolated GFP+ cells from resting muscle showed a significant reduction in miR-708 and miR-489 levels, whereas miR-92 expression (activation enriched miRNA, Fig. 1A) was strongly upregulated (Fig. 2B). In addition, a significant decrease in *Pax7* expression was noted, whereas expression of the activation (*Myod*) and differentiation (*Myogenin*) genes were strongly upregulated following AntagomiR-708 treatment (Fig. 2C). Accordingly, *in vivo* immunostaining showed that 18% of mGFP+ cells lost PAX7 expression in mice that received AntagomiR-708 during this period (Fig. 2D).

We previously showed that compromised Notch signalling *in vivo* induces satellite cells to differentiate spontaneously without entering S-phase (Mourikis et al., 2012b). However, satellite cells lacking miR-708 incorporated BrdU following activation (Fig. 2E), indicating that miR-708 knock-down induces their entry into S-phase prior to differentiation. In addition, satellite cells isolated from AntagomiR-708 treated mice exhibited premature expression of Myogenin (Fig. 2F) and consequently an increase in myotube formation as indicated by a higher fusion index (Fig. 2G). Taken together, these results indicate that reduced miR-708 levels in satellite cells leads to spontaneous exit from quiescence, activation, and premature differentiation.

Interestingly, long-term inhibition of miR-708 (28 days; Fig. 2A) showed a 50% reduction in satellite cell numbers *in vivo* (Fig. 2H and Fig. S2B). Furthermore, immunostaining with cleaved-caspase 3 showed no significant change in the number of apoptotic cells following AntagomiR-708 treatment (Fig. S2C). In contrast, numerous GFP+ fibres were observed in resting muscle indicating that mGFP+ satellite cells spontaneously fused with pre-existing myofibres (Fig. 2I). Taken together, these results demonstrate that miR-708 is necessary for maintaining satellite cell quiescence *in vivo*. Of note, transcript analysis of this residual population showed normal levels of miR-708 as well as quiescence and differentiation markers (Fig. S2D) suggesting that they escaped AntagomiR-708 treatment.

In the context of muscle damage, AntagomiR-708 treated mice displayed a slight delay in regeneration at 14 days post-injury (dpi) as indicated by smaller myofibres (Fig. S2E) however, this delay was not prominent by 31dpi (Fig. S2F). In keeping with this finding, PAX7+ cells were observed at this stage, albeit at much reduced numbers, suggesting that they were escapers. Notably, the severe defect in self-renewal of AntagomiR-

treated mice following injury and regeneration (Fig. 2J, K, S2G) indicates that miR-708 also regulates re-entry into quiescence.

miR-708 promotes satellite cell niche occupancy *in vivo* and regulates their motility and migration capacities

Suppression of miR-708 has been shown to promote invasion and metastasis of numerous cancer cells types by targeting different genes or pathways involved in the regulation of cell migration (Lin et al., 2015; Ryu et al., 2013). During homeostasis, satellite cells are localized between the myofibre membrane and the basal lamina (Sambasivan and Tajbakhsh, 2015). Surprisingly, we observed abnormal localization of PAX7+ cells in the interstitial space in the TA muscle of AntagomiR-708 treated mice (Fig. 3A) suggesting that loss of miR-708 perturbed the anchorage of satellite cells and resulted in their release from their niche.

We confirmed this phenotype by overexpressing miR-708 in freshly isolated satellite cells combined with videomicroscopy (Fig. 3B). In addition to the decrease in the number of dividing cells (Fig. 1G), the migration distance and velocity of myogenic cells treated with miR-708 were strongly diminished (Fig. 3C-D; see Supplementary Movie 1). Notably, miR-708 also altered the motility of *Odz4*-depleted satellite cells (Fig. S3A) underscoring its specific involvement in this process. Taken together, these results show that miR-708 actively inhibits the migration and motility of satellite cells.

Recently, intravital imaging showed that satellite cell properties can be monitored in vivo (Webster et al., 2016). To confirm the observed *in vitro* phenotype directly in muscle, we optimized live microscopy on freshly isolated mouse hind limb explants containing the *Extensor digitorium longus* (EDL) muscle from Scramble- or AntagomiR-treated mice using 2-photon microscopy. Intriguingly, over the 10-12h imaging period, no displacement was detected in control Scramble (n=6 mice, ≥250 cells, Fig. 3E). In contrast, miR-708 silencing *in vivo* resulted in 9% of satellite cells spontaneously exiting their niche and migrating an average distance of 8.7 ± 6.5 µm with an average velocity of 7.8 ± 4.4 nm/min (Fig. 3E, F and Supplementary Movies 2-5). These experiments provide direct evidence for a role of miR-708 as an active repressor of satellite cell migration.

To identify miR-708 putative targets, we combined three target prediction algorithms (see Fig. 3G) and identified 24 overlapping genes, among which 3 were highly expressed in activated compared to quiescent satellite cells (Liu et al., 2013): Tensin-

3 (*Tns3*), Dickkopf3 (*Dkk3*) and Syndecan-1 (*Sdc1*) (Fig. S3B). Their relevance as potential targets was tested by transfection of HEK293 cells with a luciferase reporter vector containing the 3'-untranslated region (UTR) of *Tns3*, *Dkk3* or *Sdc1* (Table S2). Notably, miR-708 repressed luciferase activity of both *Dkk3* and *Tns3*, but not *Sdc1* (Fig. 3H). Interestingly, only *Tns3* inhibition (Fig. S3C) phenocopied the overexpression of miR-708 and significantly decreased cell migration (Fig. 3I), whereas *Dkk3* knock-down showed no overt cell motility phenotype (data not shown).

Mutations in *Tns3* miRNA-binding sites significantly decreased miR-708–mediated repression (Fig. 3H), as confirmed by a Target Protector assay combined with videomicroscopy (Fig. S3D). In keeping with these observations, overexpression of TNS3 in satellite cells was sufficient to rescue the inhibition of migration mitigated by mir-708 (Fig. 3J and Supplementary Movie 6). In summary, these findings demonstrate that miR-708 exerts its repressive activity on cell migration primarily through *Tns3*.

Inhibition of Focal Adhesion Kinase represses migration and G1-S transition

Tns3 is a member of focal adhesion (FA)-associated proteins that are important regulators of cell adhesion and migration (Blangy, 2017). Moreover, the Tensin SH2 domain forms a complex with the tyrosine phosphorylated protein FAK allowing its phosphorylation and activation (Qian et al., 2009) (Fig. 4A). Notably, miR-708 overexpression in myogenic cells showed a reduction in TNS3 protein levels (Fig. 4B and S4A for antibody validation) whereas FAK phosphorylation (p-FAK) levels decreased (Fig. 4B). The presence of miR-708 did not affect the ratio of ERK/p-ERK suggesting that p-FAK was inhibited at the local level, rather than by interference of upstream effectors of the migration pathway (Fig. 4B and S4B). As observed with miR-708 gain-of-function, specific inhibition of *Tns3* resulted in downregulation of p-FAK (Fig. 4C). In contrast, the absence of miR-708 in primary satellite cells (AntagomiR), resulted in increased levels of TNS3 and p-FAK (Fig. 4D and S4C). This decrease in p-FAK was verified by immunostaining satellite cells transfected with either Mimic-708 or siTns3 (Fig. 4E-E'). Notably, temporal *in vivo* activation showed a rapid increase in *Tns3* expression within 3h following injury (Fig. S4D) and appearance of TNS3 preceded that of MYOD and cell cycle entry (Fig. S4E) indicating that release of cell migration is an early event during activation.

We note that miR-708 overexpression resulted in a delay in cell proliferation of cultured satellite cells (Fig. 1G), however, analysis of miR-708 putative targets did not identify cell cycle regulators. Thus, we propose that the inhibition of migration indirectly inhibits

cell cycle progression. To uncouple proliferation and migration properties, we induced miR-708 in cycling satellite cells isolated from Fucci-Green mice (Fluorescence ubiquitination-based cell cycle indicator), which allows temporal patterns of cell-cycle dynamics using Azami green to label S/G2/M phases (Sakaue-Sawano et al., 2008), combined with live videomicroscopy. Intriguingly, total duration of cell cycle was extended by 25% following miR-708 overexpression (Fig. 4F and Supplementary Movie 7) and this was due to a significant extension of G1 (Fig. 4G and H). These findings indicate that miR-708 exerts cell cycle regulation by modulating the G1 phase of the cell cycle.

DISCUSSION

A major question in stem cell biology is how cells enter and exit their niche, and how this interaction is stabilised to maintain the stem cell pool for extended periods. Active cell migration is a key property of satellite cells (Siegel et al., 2009), and studies have shown that stimulation of migration improves myogenic cell dispersal following transplantation, thereby resulting in enhanced engraftment efficiency (Bentzinger et al., 2014). Interestingly, it was reported that reduced levels of Fibronectin and β1-integrin during ageing results in loss of satellite cells from their niche (Lukjanenko et al., 2016) thereby underscoring the notion that multiple pathways converge to maintain the stem cell pool. However, it remains unclear how intrinsic regulators modulate the transition into and out of cellular quiescence and how cell division and migration are orchestrated with the anchoring of stem cells in their niche.

In this study, we identified miR-708 as a quiescence-specific mirtron in the *Odz4* gene, where this miRNA acts as a downstream target of Notch signalling to maintain satellite cells within their quiescent niche. Although the mechanism of action of *Odz4* has not been determined in satellite cells, it is intriguing that miR-708 is harboured within this gene, and under the regulation of Notch. Although examples of mirtrons performing regulatory functions have been reported for skeletal and cardiac muscle-specific genes (Cheung et al., 2012; van Rooij et al., 2009), here we provide the first example of such a mirtron that is under the regulation of Notch signalling, and a rare example of a miRNA that controls the maintenance of an adult stem cell population.

In silico analysis of miR-708 potential target genes identified *Tns3* that responded in functional assays to this miRNA and phenocopied the functional readouts of miR-708. The role of this Tensin isoform on cell migration is context dependent, and it can act to promote or inhibit cell mobility depending on the presence of co-factors (Qian et al.,

2009). However, our findings lead us to propose that TNS3 is maintained at low levels by the action of miR-708 in the anchored quiescent satellite cells via the inhibition of FAK. Upon activation, Notch signaling and hence miR-708 are downregulated, allowing *Tns3* to accumulate and participate in the migration of the activated cells.

Interestingly, FAK has been shown to regulate cell cycle progression by modulating the G1/S transition (Zhao et al., 1998). Therefore, we propose that indirect inhibition of FAK by miR-708 could be responsible of this extension of the G1/S transition. Our observations are concordant with a previous study showing that FAK signalling regulates cell cycle progression via the activation of *cyclin D1 (Ccnd1)* transcription through EtsB binding site of the *Ccnd1* promoter (Zhao et al., 2001).

In summary, we provide the first evidence that inhibition of the migration capacity of a stem cell is essential for maintaining the quiescent cell within its niche. We uncover a regulatory axis where Notch induces transcription of the quiescence specific mirtron miR-708 that represses Tensin3, a major component of the focal adhesion complex, to inhibit FAK activation, which in turn stabilises satellite cells within their niche. For quiescent stem cells to enter or exit their niche, they need to coordinate their final mitosis as well as cell migration. Given that satellite cells are rarely found to be subjacent, our results lead us to speculate that satellite cells continue to migrate after their last mitosis, then migration is suppressed through miR-708 as cells are then anchored in their niche. These findings suggest that mitosis and migration might be negotiated sequentially in other quiescence stem cell populations.

Acknowledgements

We would like to thank C. Akazawa, N. Suzuki, K. Ishii (Tokyo Medical and Dental University, Tokyo, Japan) for kindly providing *Odz4* KO muscle samples, O. Burri for helping with movie processing, and A. Seitz for use BIOP facilities. We thank A. Blangy for TNS3 plasmids and antibodies, Y. Wang for kindly performing some of the tail vein injections, and the Center for Translational Science, Institut Pasteur. ST acknowledges support from the Institut Pasteur, Agence Nationale de la Recherche (Laboratoire d'Excellence Revive, ANR-10-LABX-73), Association Française contre les Myopathies, CNRS, and the European Research Council (Advanced Research Grant 332893). MBB was supported by a doctoral school fellowship and Fondation pour la Recherche Médicale.

Authors contributions

S.T. and M.B.B. proposed the concept and designed the experiments. M.B.B. performed and analysed most of the experiments. D.C. performed the RNA-sequencing. D.D.G. initiated the Western Blots experiments. J.F. processed and analysed the *in vitro* videomicroscopy. P.M. generated the enhancer plasmids. B.E optimized section immunostainings and designed the cloning strategies. K.S. performed and analysed the *ex vivo* explant imaging. M.B.B. and S.T. wrote the paper. All authors read and agreed on the manuscript.

Competing Financial Interests statement

The authors declare no competing interests.

References

Baghdadi, M.B., Castel, D., Machado, L., Fukada, S.I., Birk, D.E., Relaix, F., Tajbakhsh, S., and Mourikis, P. (2018). Reciprocal signalling by Notch-Collagen V-CALCR retains muscle stem cells in their niche. Nature *557*, 714-718.

Baghdadi, M.B., and Tajbakhsh, S. (2018). Regulation and phylogeny of skeletal muscle regeneration. Dev Biol *433*, 200-209.

Bentzinger, C.F., von Maltzahn, J., Dumont, N.A., Stark, D.A., Wang, Y.X., Nhan, K., Frenette, J., Cornelison, D.D., and Rudnicki, M.A. (2014). Wnt7a stimulates myogenic stem cell motility and engraftment resulting in improved muscle strength. J Cell Biol *205*, 97-111.

Bjornson, C.R., Cheung, T.H., Liu, L., Tripathi, P.V., Steeper, K.M., and Rando, T.A. (2012). Notch signaling is necessary to maintain quiescence in adult muscle stem cells. Stem Cells *30*, 232-242.

Blangy, A. (2017). Tensins are versatile regulators of Rho GTPase signalling and cell adhesion. Biology of the cell *109*, 115-126.

Brohl, D., Vasyutina, E., Czajkowski, M.T., Griger, J., Rassek, C., Rahn, H.P., Purfurst, B., Wende, H., and Birchmeier, C. (2012). Colonization of the satellite cell niche by skeletal muscle progenitor cells depends on Notch signals. Dev Cell *23*, 469-481.

Castel, D., Baghdadi, M.B., Mella, S., Gayraud-Morel, B., Marty, V., Cavaille, J., Antoniewski, C., and Tajbakhsh, S. (2018). Small-RNA sequencing identifies dynamic microRNA deregulation during skeletal muscle lineage progression. Sci Rep *8*, 4208.

Castel, D., Mourikis, P., Bartels, S.J., Brinkman, A.B., Tajbakhsh, S., and Stunnenberg, H.G. (2013). Dynamic binding of RBPJ is determined by Notch signaling status. Genes Dev *27*, 1059-1071.

Chen, H., and Lo, S.H. (2003). Regulation of tensin-promoted cell migration by its focal adhesion binding and Src homology domain 2. The Biochemical journal *370*, 1039-1045.

Cheung, T.H., Quach, N.L., Charville, G.W., Liu, L., Park, L., Edalati, A., Yoo, B., Hoang, P., and Rando, T.A. (2012). Maintenance of muscle stem-cell quiescence by microRNA-489. Nature *482*, 524-528.

Haldar, M., Karan, G., Tvrdik, P., and Capecchi, M.R. (2008). Two cell lineages, myf5 and myf5-independent, participate in mouse skeletal myogenesis. Dev Cell *14*, 437-445.

Han, H., Tanigaki, K., Yamamoto, N., Kuroda, K., Yoshimoto, M., Nakahata, T., Ikuta, K., and Honjo, T. (2002). Inducible gene knockout of transcription factor recombination signal binding protein-J reveals its essential role in T versus B lineage decision. Int Immunol *14*, 637-645.

Hicks, C., Ladi, E., Lindsell, C., Hsieh, J.J., Hayward, S.D., Collazo, A., and Weinmaster, G. (2002). A secreted Delta1-Fc fusion protein functions both as an activator and inhibitor of Notch1 signaling. J Neurosci Res *68*, 655-667.

Ishii, K., Suzuki, N., Mabuchi, Y., Ito, N., Kikura, N., Fukada, S., Okano, H., Takeda, S., and Akazawa, C. (2015). Muscle Satellite Cell Protein Teneurin-4 Regulates Differentiation During Muscle Regeneration. Stem Cells *33*, 3017-3027.

Krutzfeldt, J., Rajewsky, N., Braich, R., Rajeev, K.G., Tuschl, T., Manoharan, M., and Stoffel, M. (2005). Silencing of microRNAs in vivo with 'antagomirs'. Nature *438*, 685-689.

Lin, K.T., Yeh, Y.M., Chuang, C.M., Yang, S.Y., Chang, J.W., Sun, S.P., Wang, Y.S., Chao, K.C., and Wang, L.H. (2015). Glucocorticoids mediate induction of microRNA-708 to suppress ovarian cancer metastasis through targeting Rap1B. Nature communications *6*, 5917.

Liu, L., Cheung, T.H., Charville, G.W., Hurgo, B.M., Leavitt, T., Shih, J., Brunet, A., and Rando, T.A. (2013). Chromatin modifications as determinants of muscle stem cell quiescence and chronological aging. Cell Rep *4*, 189-204.

Livak, K.J., and Schmittgen, T.D. (2001). Analysis of relative gene expression data using real-time quantitative PCR and the 2(-Delta Delta C(T)) Method. Methods *25*, 402-408.

Lukjanenko, L., Jung, M.J., Hegde, N., Perruisseau-Carrier, C., Migliavacca, E., Rozo, M., Karaz, S., Jacot, G., Schmidt, M., Li, L.*, et al.* (2016). Loss of fibronectin from the aged stem cell niche affects the regenerative capacity of skeletal muscle in mice. Nat Med *22*, 897-905.

Mourikis, P., Gopalakrishnan, S., Sambasivan, R., and Tajbakhsh, S. (2012a). Cell-autonomous Notch activity maintains the temporal specification potential of skeletal muscle stem cells. Development *139*, 4536-4548.

Mourikis, P., Sambasivan, R., Castel, D., Rocheteau, P., Bizzarro, V., and Tajbakhsh, S. (2012b). A critical requirement for notch signaling in maintenance of the quiescent skeletal muscle stem cell state. Stem Cells *30*, 243-252.

Murtaugh, L.C., Stanger, B.Z., Kwan, K.M., and Melton, D.A. (2003). Notch signaling controls multiple steps of pancreatic differentiation. Proc Natl Acad Sci U S A *100*, 14920-14925.

Muzumdar, M.D., Tasic, B., Miyamichi, K., Li, L., and Luo, L. (2007). A global double-fluorescent Cre reporter mouse. Genesis *45*, 593-605.

Qian, X., Li, G., Vass, W.C., Papageorge, A., Walker, R.C., Asnaghi, L., Steinbach, P.J., Tosato, G., Hunter, K., and Lowy, D.R. (2009). The Tensin-3 protein, including its SH2 domain, is phosphorylated by Src and contributes to tumorigenesis and metastasis. Cancer cell *16*, 246-258.

Rocheteau, P., Gayraud-Morel, B., Siegl-Cachedenier, I., Blasco, M.A., and Tajbakhsh, S. (2012). A subpopulation of adult skeletal muscle stem cells retains all template DNA strands after cell division. Cell *148*, 112-125.

Ruby, J.G., Jan, C.H., and Bartel, D.P. (2007). Intronic microRNA precursors that bypass Drosha processing. Nature *448*, 83-86.

Ryu, S., McDonnell, K., Choi, H., Gao, D., Hahn, M., Joshi, N., Park, S.M., Catena, R., Do, Y., Brazin, J.*, et al.* (2013). Suppression of miRNA-708 by polycomb group promotes metastases by calcium-induced cell migration. Cancer cell *23*, 63-76.

Sakaue-Sawano, A., Kurokawa, H., Morimura, T., Hanyu, A., Hama, H., Osawa, H., Kashiwagi, S., Fukami, K., Miyata, T., Miyoshi, H.*, et al.* (2008). Visualizing spatiotemporal dynamics of multicellular cell-cycle progression. Cell *132*, 487-498.

Sambasivan, R., Gayraud-Morel, B., Dumas, G., Cimper, C., Paisant, S., Kelly, R.G., and Tajbakhsh, S. (2009). Distinct regulatory cascades govern extraocular and pharyngeal arch muscle progenitor cell fates. Dev Cell *16*, 810-821.

Sambasivan, R., and Tajbakhsh, S. (2015). Adult skeletal muscle stem cells. Results and problems in cell differentiation *56*, 191-213.

Seale, P., Sabourin, L.A., Girgis-Gabardo, A., Mansouri, A., Gruss, P., and Rudnicki, M.A. (2000). Pax7 is required for the specification of myogenic satellite cells. Cell *102*, 777-786.

Shinin, V., Gayraud-Morel, B., Gomes, D., and Tajbakhsh, S. (2006). Asymmetric division and cosegregation of template DNA strands in adult muscle satellite cells. Nat Cell Biol *8*, 677-687.

Siegel, A.L., Atchison, K., Fisher, K.E., Davis, G.E., and Cornelison, D.D. (2009). 3D timelapse analysis of muscle satellite cell motility. Stem Cells *27*, 2527-2538.

Tinevez, J.Y., Perry, N., Schindelin, J., Hoopes, G.M., Reynolds, G.D., Laplantine, E., Bednarek, S.Y., Shorte, S.L., and Eliceiri, K.W. (2017). TrackMate: An open and extensible platform for single-particle tracking. Methods *115*, 80-90.

van Rooij, E., Quiat, D., Johnson, B.A., Sutherland, L.B., Qi, X., Richardson, J.A., Kelm, R.J., Jr., and Olson, E.N. (2009). A family of microRNAs encoded by myosin genes governs myosin expression and muscle performance. Dev Cell *17*, 662-673.

Webster, M.T., Manor, U., Lippincott-Schwartz, J., and Fan, C.M. (2016). Intravital Imaging Reveals Ghost Fibers as Architectural Units Guiding Myogenic Progenitors during Regeneration. Cell stem cell *18*, 243-252.

Zammit, P.S., Golding, J.P., Nagata, Y., Hudon, V., Partridge, T.A., and Beauchamp, J.R. (2004). Muscle satellite cells adopt divergent fates: a mechanism for self-renewal? J Cell Biol *166*, 347-357.

Zhao, J., Pestell, R., and Guan, J.L. (2001). Transcriptional activation of cyclin D1 promoter by FAK contributes to cell cycle progression. Molecular biology of the cell *12*, 4066-4077.

Zhao, J.H., Reiske, H., and Guan, J.L. (1998). Regulation of the cell cycle by focal adhesion kinase. J Cell Biol *143*, 1997-2008.

Figure legends

Fig. 1. miR-708, a Notch pathway target mirtron specifically expressed in quiescent satellite cells, suppresses proliferation and differentiation while its inhibition impairs self-renewal.

(A) Gene expression from RNA deep sequencing of freshly isolated satellite cells from *Tg:Pax7-nGFP* adult mice (QSC, n=2), *in vitro* activated satellite cells for 60h (ASC, n=3) and differentiated cells cultured for 7 days (DIFF, n=2).

(B) ChIP-seq tracks showing NICD/RBPJ occupancy on enhancers associated with mouse *Odz4* locus. Orange rectangle indicates RBPJ binding positions.

(C) Transcriptional response measured by Firefly luciferase signal of two enhancers of *Odz4* to activation of Notch signalling in C2C12 cells cultured on Dll1-Fc. Control Fc is set at 1; n=3 independent assays.

(D) RT-qPCR analysis of miR-708 in Control (*Tg:Pax7-CT2; Rbpj*$^{+/+}$) and *Rbpj* conditional KO (*Rbpj* null; *Tg:Pax7-CT2; Rbpj*$^{flox/flox}$) satellite cells isolated from resting muscles.

(E) Induction of miR-708 in E14.5 control (*Myf5*$^{Cre/+}$*; R26*$^{mTmG/+}$) and *Myf5*^{Cre}*-NICD* (*Myf5*$^{Cre/+}$*; R26*$^{stop\text{-}NICD\text{-}nGFP/+}$) myogenic cells isolated by FACS, assessed by RT-qPCR. let-7e is not a Notch target; n=4 mice or fetuses/genotype.

(F) Transcript expression levels of miR-708 targeted by Notch in cells fractionated by FACS based on GFP-intensity from *Tg:Pax7-nGFP* mice at 8 postnatal day (P8): Pax7^{High} (20%), Pax7^{Mid} (40%) and Pax7^{Low} (20%); n=3 pups.

(G) EdU reaction and GFP staining of satellite cells isolated from *Tg:Pax7-nGFP* mice 24h after Mimic-708 or Control (Ctr) transfection. Time course of proliferation by quantification of EdU 24h to 4days following miR-708 overexpression (Mimic-708) or Control.

(H) Myogenin staining of satellite cells isolated from *Tg:Pax7-nGFP* mouse 72h after Mimic-708 or control Scramble transfection. Quantification of Myogenin+ cells at 72h and 4 days following treatment; n=4 mice, ≥400 cells, 2 wells/condition.

(I) miR-708 knock-down using AntimiR-708 transfection of single EDL myofibres from *Tg:Pax7-nGFP* mice cultured for 72h and immunostained for GFP and Myogenin. Quantification of PAX7^{+}/MYOG^{-} (21% *vs.* 5%), PAX7^{-}/MYOG^{-} (36% *vs.* 15%) and PAX7^{-}/MYOG^{+} (43% *vs.* 79% for Scramble and AntimiR-708 respectively) populations; 4 mice/condition, n=25 fibres.

(J) Satellite cells isolated by FACS from control and *Odz4* null mice, treated with Mimic or Control for 72h and stained for Myogenin. Quantification of Myogenin+ cells; n=3 mice/condition, ≥250 cells.

Error bars, mean ± SD; two-sided unpaired t-test; #p-value: two-sided paired t-test. Scale bar: 50µm. See also Supplementary Figure S1.

Fig. 2. miR-708 maintains the satellite cell quiescent state.

(A) Experimental scheme of tamoxifen, AntagomiR and BrdU administration to *Tg:Pax7-CT2; R26^{mTmG}* mice. AntagomiR-708 and Scramble control were injected every day in the tail vein for 4 days after the end of tamoxifen treatment (D0) and mice were analysed 10 days (B-G) and 28 days (H-I) post-treatment.

(B) miRNA expression in control (Scramble) and miR-708 knock-down (AntagomiR-708) cells isolated by FACS 10 days post-treatment.

(C) mRNA expression in control and AntagomiR-708 cells isolated by FACS 10 days post-treatment.

(D) Representative images of satellite cells on *Tibilias anterior* muscle section from Scramble and AntagomiR-708 treated mice stained for membrane-GFP and PAX7. Quantification of mGFP+/PAX7- cells (arrow) relative to total mGFP+ cells; n=4 mice/treatment.

(E) membrane-GFP+ satellite cells on TA muscle section from Scramble and AntagomiR-708 treated mice stained for BrdU. Quantification of mGFP+/BrdU+ cells relative to total mGFP+ cells. Asterisk shows mGFP-/BrdU+ cells; arrows indicate mGFP+/BrdU+ cell; n=4 mice/treatment.

(F) Myogenin and GFP immunostainings of satellite cells cultured for 72h and quantification; n=3 mice/treatment; ≥150 cells.

(G) Myosin Heavy Chain (MyHC) staining of satellite cells from Scramble and AntagomiR-708 treated mice isolated by FACS, cultured for 5 days and quantification of fusion index (nuclei in MyHC+ myotubes with ≥2 nuclei/total number of nuclei); n=3 mice/treatment, ≥500 nuclei, 2 wells/condition.

(H) Laminin and PAX7 immunostaining on quiescent TA muscle section from Scramble and AntagomiR-treated mice (10dpa) and quantification of PAX7^{+} cells/mm^{2}; n=6 Scramble and n= 8 AntagomiR treated mice.

(I) Immunostaining for Laminin and GFP on sections from TA muscles of mice 28 days post-Scramble and AntagomiR-708 treatment, inset shows whole TA section.

(J) Schemes of *Tg:Pax7-CT2; R26^{mTmG}* mice fed with tamoxifen for 2 weeks, injured with Cardiotoxin (CTX) at D0 followed by daily AntagomiR-708, or Scramble injections for 4 days. Muscles were collected 14 days post-injury.

(K) Laminin and PAX7 immunostaining on injured TA muscle section from Scramble and AntagomiR-treated mice (14 days post-injury) and quantification of PAX7^{+} cells/mm^{2}; n=3 Scramble and n= 4 AntagomiR treated mice.

Error bars, mean ± SD; two-sided unpaired t-test. Scale bar: 25µm (D, F), 50µm (E, G, H, K), 100µm and 300µm in inset (I). See also Supplementary Figure S2.

Fig. 3. miR-708 regulates myogenic cell migration and motility.

(A) Immunostaining for Laminin and PAX7 on sections from resting TA muscles 10 days post Scramble and AntagomiR-708 treatment and quantification of PAX7+ cells in interstitial space (2% for Scramble vs. 38% for AntagomiR-708); n=4 mice; 2 sections/TA.

(B) Scheme of miR-708 overexpression on membrane-GFP+ satellite cells isolated from *Tg:Pax7-CT2; R26*^{mTmG} mice treated 2 weeks with tamoxifen.

(C) Maximum projection of 48h-time-lapse experiment of mGFP+ cells overexpressing miR-708 (Mimic-708) and Control. Coloured line depicts trajectory of a cell for every condition. See Supplementary Movie 1.

(D) Distance and velocity of miR-708 overexpressing cells (Mimic-708) and control were scored for 48h; n=30 cells.

(E) Maximum projection of EDL muscle from Scramble or AntagomiR-708 treated mice imaged on an explant at 0h and 12h (n=6 mice/treatment). Arrows point tracked cells. See Supplementary Movies 2-5.

(F) Migration distance of *in vivo* AntagomiR or Scramble-treated satellite cells on an explant imaged for 12h (0 cells displace in Scramble vs. 13 cells in AntagomiR); n=6 mice/treatment; n=250 cells tracked.

(G) Venn Diagram displaying putative targets of miR-708 as predicted by TargetScan, TargetRank and MiRDB.

(H) Schemes of *Tns3* (*Tensin-3*), *Dkk3* (*Dickkopf-3*), *Sdc1* (*Syndecan-1*) constructs and mutated *Tns3* 3'UTR with relative luciferase activity associated with each in presence (Mimic-708) or absence (Mimic-Ctr) of miR-708. Note, analysis using full 3'UTR length of *Sdc1* and *Dkk3* and truncated *Tns3* 3'UTR; n=6 independent experiments, 2 wells/condition.

(I) Migration properties assessed by transwell assay, of miR-708-overexpressing (Mimic-708) or upon Tns3 knock-down (siTns3) compared to control: Mimic-Ctr, and siCtr respectively. Quantification of number of migrating satellite cells through pores of the membrane upon treatment; n=4 mice, 2 fields counted/membrane.

(J) Velocity delayed in presence of miR-708 is rescued by overexpression of TNS3. See Supplementary Movie 6.

Error bars, mean ± SD; two-sided unpaired t-test (A), Fisher (F), Mann-Whitney test (H, J), two-sided paired t-test (I). Scale bar: 50µm (A-C), 20µm (E) and 10µm (A inset and I). See also Supplementary Figure S3.

Fig. 4. Tensin-3 inhibition reduces FAK activation and phenocopies miR-708 overexpression.

(A) Signaling pathway for cell migration mediated by ERK. Growth factors (PDGF, EGF and FGF) trigger downstream signaling Ras-Raf-MEK that further activate ERK. Activated ERK regulates focal adhesion dynamics by phosphorylation of FAK and Paxillin. Tensin-3 can interact with FAK (Chen and Lo, 2003).

(B) Western blot showing protein levels and phosphorylation state of FAK, TNS3, Paxillin and ERK after miR-708 overexpression (Mimic-708) and Control (Ctr) in C2C12 myoblasts; n=4 independent experiments.

(C) Protein levels and phosphorylation of FAK upon *Tns3* knock-down (siTns3) in C2C12 cells; n=4 independent experiments.

(D) TNS3 and p-FAK protein levels in freshly isolated satellite cells from Scramble and AntagomiR-treated mice.

All Western-blots were normalized to GAPDH levels; n=3-4 mice/condition.

(E-E') Actin staining with Phalloidin and immunostaining of p-FAK on satellite cells isolated from *Tg:Pax7-nGFP* mouse and transfected with Mimic-708 (E) or siTns3 (E'). Arrowheads show p-FAK positive signal. Two fields from the same culture dish are shown, separated by line; n=4 mice/condition.

(F) Cell cycle duration (hours) of satellite cells isolated from Fucci-green mouse treated with Mimic-708 or control and tracked for one division.

(G) Cell cycle repartition of Fucci-green satellite cell following control and miR-708 overexpression (Mimic-708). Cells were tracked for one cell cycle.

(H) Time series of a Fucci-green satellite cell transfected with Mimic-708 or control with corresponding kymograph. Distance between two arrows represents one cell cycle; n=3 mice, 15 cells tracked/condition. See Supplementary Movie 7.

Error bars, mean ± SD; two-sided unpaired t-test (B-D); Mann-Whitney test (F-G). Scale bar: 25µm. See also Supplementary Figure S4.

STAR Methods

CONTACT FOR REAGENT AND RESOURCE SHARING

Further information and requests for resources and reagents should be directed to and will be fulfilled by the Lead Contact, Shahragim Tajbakhsh (shahragim.tajbakhsh@pasteur.fr).

EXPERIMENTAL MODEL AND SUBJECT DETAILS

Animals

Animals housing, husbandry and handling were performed in the animal facility of Institut Pasteur in accordance with the national and European community guidelines. The health and immune status of all mice used were normal, and they were not involved in any previous procedures. Food and water were administered *ad libitum*. For Notch *in vivo* gain-of-function, *Myf5*^{Cre} mice (Haldar et al., 2008) were crossed with *R26*$^{stop\text{-}NICD\text{-}nGFP}$ (Murtaugh et al., 2003), and fetuses were recovered 14.5 days post-fertilization. For Notch *in vivo* knock-down, *Tg:Pax7-CreERT2* (Mourikis et al., 2012b) was crossed with *Rbpj*$^{flox/flox}$ (Han et al., 2002) and the lineage tracing mouse line *R26*^{mTmG} (Muzumdar et al., 2007). The *Tg:Pax7-nGFP* mouse line was generated in the Tajbakhsh lab (Sambasivan et al., 2009) with a BAC containing approximately 200 kbp of mouse genomic DNA including the locus encoding *Pax7* and sequences both upstream (~55 kbp with respect to Pax7 initiator ATG) and downstream (~60 kbp from terminator codon). The targeting vector was designed to introduce nGFP (nuclear GFP) into the first exon of Pax7 gene (mutated initiator ATG and deleted bases 58-94 of exon 1). *Odz4* KO mice were kindly provided by Drs. Chihiro Akazawa and Nobuharu Suzuki (Ishii et al., 2015) and Fucci-Green mice (Sakaue-Sawano et al., 2008) by Dr. Atsushi Miyawaki. All experiments were performed indistinguishably with mice of both sexes from 6 to 8 weeks of age. All protocols were approved by ethics committee at Institut Pasteur and the French Ministry.

METHOD DETAILS

Muscle injury, tamoxifen and BrdU administration

For muscle injury, mice were anesthetized with 0.5% Imalgene/2% Rompun and the TA muscle was injected with 50*µ*l of Cardiotoxin (10mM; Latoxan, L8102). *Tg:Pax7-CreERT2; Rbpj*^{flox}*; R26*^{mTmG} and *Tg:Pax7-CreERT2; R26*^{mTmG} were fed with tamoxifen containing diet for two weeks (Envigo, TD55125). Five days prior sacrifice mice were given the thymidine analogue 5-Bromo-2'-deoxyuridine (BrdU, 0.5mg/ml, Sigma, B5002) in the drinking water supplemented with sucrose (25mg/ml). Comparisons were done between age-matched littermates using 8-12-week old mice.

Satellite cell dissociation and fluorescence activated cell sorting (FACS)

Adult and foetal limb muscles were dissected, minced and incubated with a mix of Dispase II (Roche, 04942078001) 3U/ml, Collagenase A (Roche, 11088793001) 100ug/ml and DNase I (Roche, 11284932001) 10mg/ml in Hank's Balanced Salt Solution (HBSS, Gibco) supplemented with 1% Penicillin-Streptomycin (PS; Gibco) at 37°C at 60rpm in a shaking water bath for 2h. The muscle suspension was successively filtered through 100µm and 70µm cell strainers (Milteny, 130-098-463 and 130-098-462) and then spun at 50g for 10min at 4°C to remove large tissue fragments. The supernatant was collected and washed twice by centrifugation at 600g for 15min. Prior to FACS, the final pellet was resuspended in cold Dulbecco's Modified Eagle Medium (DMEM, Gibco) supplemented with 1%PS and 2% Fetal Bovine Serum (FBS, Gibco) and the cell suspension was filtered through a 40µm strainer (BD, 352340).

For satellite cell isolation from Fucci-green and *Odz4* KO mice, cells were stained with α7-integrin-APC (Ablab, clone R2F2, 1/1000), CD34-e450 (eBioscience, clone RAM34, 1/50), Sca1-Pe-Cy7 (eBioscience, clone D7, 1/400), CD45-Pe-Cy7 (eBioscience, clone 30-F11, 1/100) and CD31-PE (BD, clone MEC13.3, 1/50). Satellite cells were sorted with an Aria III (BD Biosciences).

RNA extraction and quantitative PCR (RT-qPCR)

Micro-RNAs from cells or tissue were purified using (Qiagen miRNAeasy® Micro Kit) and reverse transcribed in cDNA using miRCURY LNA® universal RT kit (Exiqon, 203301). Expression of mature miRNAs was determined using ExiLENT SYBR® green master mix (Exiqon) and miRNA LNA™ PCR primers (Exiqon; hsa-miR-708-5p, 204490; mmu-miR-489-3p, 205036; hsa-let-7e-5p, 205711; mmu-miR-92-5p, 205947). Two snoRNA; RNU5G (Exiqon, 308014) and SNORD65 (Exiqon, 308016) were used for normalization.

Total mRNAs were isolated using (Qiagen RNAeasy® Micro Kit) and reverse transcribed using SuperScriptIII® enzyme (Invitrogen, 18080093). The eventual remaining RNAs were degraded by incubation 20 min at 37°C with RNase H endonuclease (Roche, 10786357001). Expression of mature mRNAs was assessed with SYBR green master mix (Roche, 04913914001) and analysis were performed using the $2^{-\Delta\Delta CT}$ method (Livak and Schmittgen, 2001). All RT-qPCR samples were normalized with *Tbp* and *Rpl13*. Specific forward and reverse primers used for RT-qPCR are listed in Table S1.

Satellite cell culture and transfection

Satellite cells were isolated by FACS, and total muscle preparations were seeded at $3x10^3$ cells/cm^2 on Matrigel® (Corning, 354248) coated dishes for 30 min at 37°C. Cells were cultured

in a growth medium (GM) containing DMEM/F12 (50:50; Gibco), 1% PS, 20% FBS, 2% Ultroser (Pall, 15950-017) and incubated at 37°C, 3% O_2, 5% CO_2 for the indicated time. Half of the medium was changed every 3 days. To assess proliferation, cells were pulsed with the thymidine analogue 5-ethynyl-2′-deoxyuridine (EdU), $1x10^{-6}$ M, 2h prior to fixation (ThermoFisher Click-iT Plus EdU kit, C10640).

Freshly isolated satellite cells from *Tg:Pax7-nGFP* were transfected in suspension with miRIDIAN microRNA mmu-miR-708-5p mimic (AAGGAGCUUACAAUCUAGCUGGG, Dharmacon, C310987) and Scramble Control#1 (UCACAACCUCCUAGAAAGAGUAGA; Dharmacon, CN-001000) at 200nM final concentration using Lipofectamine 2000 (ThermoFisher, 11668) in Opti-MEM (Gibco). Four hours after transfection, 3 volumes of fresh growth medium were added and cells were cultured for the indicated time. Cells were fixed with 4% paraformaldehyde (PFA) in PBS 10 min at room temperature (RT).

Single myofibre isolation and antimir transfection

Single myofibres were isolated from *Extensor digitorum longus* (EDL) muscles following the previously described protocol (Shinin et al., 2006). Briefly, EDL muscles were dissected and incubated in 0.1% w/v collagenase (Sigma, C0130)/DMEM for 1h in a 37°C shaking water bath at 40rpm. Following enzymatic digestion, mechanical dissociation was performed to release individual myofibres that were then transferred to serum-coated petri dishes. Single myofibres were transfected with miRCURY LNA™ mmu-miR-708-5p inhibitor (AAGGAGCUUACAAUCUAGCUGGG, Exiqon, 4101225) or Scramble Control A (Exiqon, 199096) at a final concentration of 250nM, using Lipofectamine 2000 (ThermoFisher, 11668) in Opti-MEM (Gibco). Four hours after transfection, 6 volumes of fresh satellite cell growth medium was added and fibres were cultured for 72h at 37°C, 3%O_2. Fibres were fixed with 4%PFA/PBS 15 min at room temperature.

Immunostaining of cells, myofibres and sections

Following fixation, cells and myofibres were washed three times with PBS, then permeabilised and blocked at the same time in buffer containing 0.25% Triton X-100 (Sigma), 10% goat serum (GS; Gibco) for 30min at RT. For BrdU immunostaining, epitopes were unmasked with DNase I (1000 U/ml, Roche, 04536282001) for 30 min at 37°C. Cells and fibres were then incubated with primary antibodies overnight at 4°C. Samples were washed with 1X PBS three times and incubated with Alexa-conjugated secondary antibodies (Life Technologies, 1/1000) and Hoechst (Life Technologies, 1/10000) for 45 min at RT. EdU staining was chemically revealed using the Click-iT Plus kit according to manufacturer's recommendations (Life Technologies, C10640). For Phalloidin staining, cells were fixed in 3%PFA/2% Sucrose for 15

min at RT, permeabilised with 0.1% Triton for 10 min and incubated with Rhodamine Phalloidin for 30 min at RT.

Isolated *Tibialis anterior* (TA) muscles were frozen in liquid-nitrogen cooled isopentane and sectioned transversely at 8µm. Sections were post-fixed with 4%PFA overnight at 4°C and washed 3 times with 1X PBS. For antibody staining of transcription factors, antigen retrieval was performed by incubating sections in boiling 10mM Tris-EDTA buffer pH9 in a 2100 Retriver device.

Confocal images were acquired with Zeiss LSM700 microscope and Zen Blue 2.0 software. Quantifications were done on the whole TA muscle section taken from two distally located regions in the muscle for each mouse acquired with Zeiss Axioscan Z1.

AntagomiR synthesis and administration

AntagomiR and Scramble were designed as described before (Krutzfeldt et al., 2005). PAGE-purified AntagomiR were synthetized with the following modifications (Dharmacon):

AntagomiR-708:

5'mC*mC*mCmAmGmCmUmAmGmAmUmUmGmUmAmAmGmCmU*mC*mU*mU*3'-Chl;

Scramble:

5'mU*mU*mUmCmUmAmAmUmCmAmAmGmGmGmUmCmUmGmUmG*mG*mC*mU*3'-Chl. Where * represents phosphothiotate linkage at given position; m, 2'OMethyl-modified nucleotides; Chl, cholesterol linked through a hydroxyprolinol linkage. AntagomiR molecules were resuspended in saline and injected every day for 4 days into tail veins at a dose of 8µg/g of mouse.

Transwell Assay

The bottom part of a transwell membrane with 8µm pores size (Corning, 3428) was coated with Matrigel 15min at 37°C. FACS isolated satellite cells from *Tg:Pax7-nGFP* mouse were culture as described before for 24h prior to Mimic or siRNA transfection. Twenty-four hours (for Mimic) or 48h (for siRNA) post-transfection, myogenic cells where trypsinized (Gibco, 25200) 10 min at 37°C. Trypsin was washed away by the addition of DMEM/10% FCS and cells were centrifuged 15min at 600g. Cell pellets were resuspended in a low serum medium DMEM/2% FCS and seeded on the upper part of the transwell. Cells were allowed to migrate in a vertical direction through the pores of the membrane into the lower compartment, in which higher serum content was present (growth medium). Six hours after seeding, the membrane was fixed 15min with methanol and non-migrated cells remaining on the topside of the filter were removed with a cotton swab. The migrated cells were stained with Crystal Violet 0.5%/ 25% Methanol for 5min (Sigma, C0775) and washed 5 times in 1X PBS.

Construction of luciferase reporters, mutagenesis and luciferase assays

For the generation of luciferase reporters, candidate enhancers of *Odz4* were amplified by PCR from genomic DNA of C2C12 cells. The enhancers were then cloned into the firefly-luciferase pGL3-Basic vector (Promega, E1751) upstream of a minimal thymidine kinase promoter (minTK) as described previously (Castel et al., 2013). Twenty-four hours after transfection, C2C12 cells were trypsinized and plated on Dll-Fc or control Fc for 24h before luciferase activity measurement. For Dll1-Fc and Fc protein production, conditioned medium was prepared from stable 293T cell lines, transfected with the corresponding plasmid as previously described (Hicks et al., 2002).

The full 3'UTR length of mouse *Dkk3* (2.5kb) and *Sdc1* (1.8kb) (http://genome.ucsc.edu) were amplified by PCR from reverse transcribed cDNA from total RNA extract of E17.5 mouse foetuses (Table S2). Partial *Tns3*-3'UTR (500bp) containing miR-708 potential binding site of interest was obtained from SourceBioscience (EST clone: IMAGp998D088514Q) (Table S2). 3'UTR were cloned in the pGL3-Control vector (Promega, E1741) at the XbaI site downstream of the luciferase gene. Targeted mutagenesis was performed using the Q5® site-directed mutagenesis kit (NEB, E0554S) according to manufacturer's guidelines. HEK293T were co-transfected with the plasmid of interest and Mimic-708 or Scramble negative control and cultured in DMEM/10%FCS, at 37°C, 5% CO_2, and 20% O_2 for 48h before luciferase assay. In both assays, a Renilla luciferase plasmid (pCMV-Renilla) was also co-transfected as transfection control and empty pGL3 vector was used as a background negative control. Firefly and renilla luciferase activities were detected with Dual Glo® luciferase assay system (Promega, 2920) and the results were expressed as firefly luciferase activity relative to Renilla luciferase activity.

Target Protector assay

Freshly isolated satellite cells from *Tg:Pax7-nGFP* mice were transfected using miScript Target Protector according to the manufacturer's recommendation (Qiagen, 219000). Briefly, Script Target Protector (10nM final) and miRNA Mimic (500nM final) were transfected using Lipofectamine 2000 as described above.

Western Blot

C2C12 cells were transfected with Mimic (final concentration 200nM) or siRNA (siTns3 #L063982, siDkk3 #L060631, Scramble #D0018100205, Dharmacon, final concentration 250nM) as described above and cultured in DMEM/10%FCS, at 37°C, 5% CO_2, and 20% O_2 for 48h. Primary satellite cells were sorted directly in lysis buffer (150M NaCl, 50mM Tris pH8, 5mM EDTA, 1% NP-40 (Sigma, I8896), 0.5% sodium deoxycholate, 0.1% SDS supplemented with 1X proteases (Sigma, S8820) and phosphatases (Roche, 4906845001) inhibitors) and

$5x10^4$ cells were loaded/lane. Total protein extracts were run on a 4-12% Bis-Tris Gel NuPAGE (Invitrogen, NP0322) and transferred on a PVDF Amersham Hybond-P transfer membrane (Ge Healhcare, RPN303F). The membrane was then blocked with 5% BSA (Sigma, A9418) in Tris-Buffer Saline (TBS) for 1h at RT and probed with specific primary antibodies overnight at 4°C. After three washes in TBS1X-Tween 0.2%, membrane was incubated with HRP-conjugated goat anti-rabbit (1:3000, Pierce, 31460) or anti-mouse (1:10000, Pierce, 31430) IgG secondary antibodies, and revealed by chemiluminescence (Pierce ECL2 western blotting substrate, Thermo Scientific, 80196). All Western blots bands were quantified using ImageJ software.

Ex vivo videomicroscopy

Cells were transfected and seeded as indicated above. The plate was then incubated at 37°C, 5% CO_2, and 3% O_2 (Zeiss, Pecon). A Zeiss Observer.Z1 connected to an LCI PlnN 10×/0.8 W objective and Hamamatsu Orca Flash 4 camera piloted with Zen (Zeiss) was used. Cells were imaged every 13 min for the time indicated. Distance and velocity plots were obtained using the Manual tracking plugin available in Fiji (Fig. 3D) or automatic tracking (remaining experiments) provided by TrackMate (Tinevez et al., 2017) after contrast enhancement using a median filter followed by “Detect Edges” functions available in FIJI. Track parameters were kept within the same datasets; track segment splitting was allowed with a maximal distance between time frames of 50µm. For the kymograph, cells were manually tracked and a fixed ROI of 150px by 150px containing the cell in its center was extracted for each timepoint. A line encompassing the cell nucleus was drawn and the Dynamic Reslice plugin in Fiji was used to obtain the corresponding kymograph.

Live videomicroscopy of muscle explants

Live imaging was performed on the *Extensor digitorum longus* (EDL) in an explant culture system. The EDL was kept attached to the bone from tendons on both sides while the remaining leg muscles were carefully removed. The explant was immobilized on a 50mm glass bottom dish (Mattek Co, P50G-0-30-F) coated with 1% low melting agarose (Sigma, A9414) and cultured in satellite cell GM supplemented with 20mM $NaHCO_3$ at 37°C, 5% CO_2. Imaging was conducted on a Zeiss LSM7MP microscope with a 2-photon laser (Chameleon Laser from Coherent) at 860nm and a Zeiss Plan-Apochromat 20x/0.8 M27 objective. Z stacks of 160-200 um were acquired with a step of 2.5 µm. GFP and tdTomato were simultaneously detected using 2 NDD detectors with the following bandpass filters: BP 575-610 and BP 640-710. Movies had a duration of 10-12h with a 30min interval. A maximum intensity projection (MIP) of all optical sections was done using Zen Blue software from Carl Zeiss. The “Correct 3D drift”

plugin available in Fiji was then applied to the MIP and afterwards the “Manual Tracking” plugin in Fiji was employed to obtain the relevant data (velocities and distance).

QUANTIFICATION AND STATISTICAL ANALYSIS

Statistical analysis

No statistical methods were used to predetermine sample size. The investigators were not blinded to allocation during experiments and outcome assessment. No animal has been excluded from analysis and no randomization method has been applied in this study. For comparison between two groups, two- tailed paired, unpaired Student’s t-tests or Mann-Whitney test were performed to calculate P values and to determine statistically significant differences. The number of independent experimental replications (n value ≤ 3: mice, fetuses, experiments, wells or counted cells/muscles), the definition of center, variation (mean ± SD) and statistical test (P value) are reported in each corresponding figure legend. Fisher test was used to compare phenotypic variations in Fig. 3F. All statistical analyses were performed with GraphPad Prism software.

Data and software availability

The small RNA-seq are available in the ArrayExpress database at EMBL-EBI under accession no. E-MTAB-5955 (Castel et al., 2018). Notch ChIP-seq data are available under the accession no. GEO Accession no. GSE37184 (Castel et al., 2013). Microarray analysis on freshly isolated and activated satellite cells data are available under the GEO accession no. GSE52192 (Liu et al., 2013). Supplementary movies are available at http://dx.doi.org/10.17632/xhrjsbwg92.1#folder-16a2cd73-967e-4fda-9fb8-a2009a1cf4fa.

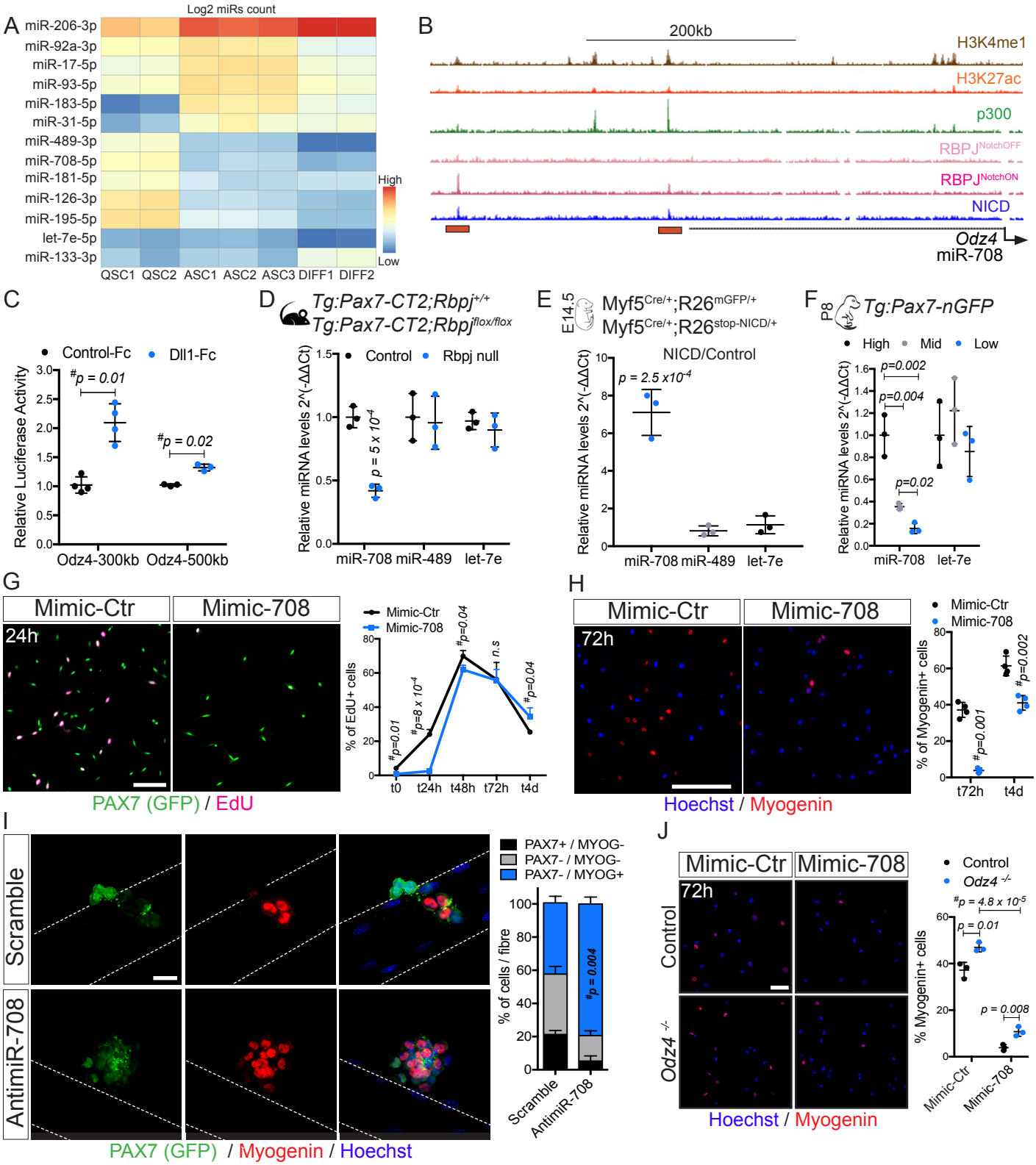
A
Log2 miRs count
miR-206-3p
miR-92a-3p
miR-17-5p
miR-93-5p
miR-183-5p
miR-31-5p
miR-489-3p
miR-708-5p
miR-181-5p
miR-126-3p
miR-195-5p
let-7e-5p
miR-133-3p
High
Low
QSC1 QSC2 ASC1 ASC2 ASC3 DIFF1 DIFF2
B
200kb
H3K4me1
H3K27ac
p300
RBPJNotchOFF
RBPJNotchON
NICD
Odz4
miR-708
C
Control-Fc
Dll1-Fc
Relative Luciferase Activity
#p = 0.01
#p = 0.02
Odz4-300kb Odz4-500kb
D
Tg:Pax7-CT2;Rbpj+/+
Tg:Pax7-CT2;Rbpjflox/flox
Control
Rbpj null
Relative miRNA levels 2^(-ΔΔCt)
p = 5 x 10-4
miR-708 miR-489 let-7e
E
E14.5
Myf5Cre/+;R26mGFP/+
Myf5Cre/+;R26stop-NICD/+
NICD/Control
p = 2.5 x10-4
Relative miRNA levels 2^(-ΔΔCt)
miR-708 miR-489 let-7e
F
P8
Tg:Pax7-nGFP
High Mid Low
p=0.002
p=0.004
p=0.02
Relative miRNA levels 2^(-ΔΔCt)
miR-708 let-7e
G
Mimic-Ctr
Mimic-708
24h
PAX7 (GFP) / EdU
Mimic-Ctr
Mimic-708
% of EdU+ cells
#p=0.01
#p=8 x 10-4
#p=0.04
n.s
#p=0.04
t0 t24h t48h t72h t4d
H
Mimic-Ctr
Mimic-708
72h
Hoechst / Myogenin
Mimic-Ctr
Mimic-708
% of Myogenin+ cells
#p=0.001
#p=0.002
t72h t4d
I
Scramble
AntimiR-708
PAX7+ / MYOG-
PAX7- / MYOG-
PAX7- / MYOG+
% of cells / fibre
#p = 0.004
Scramble
AntimiR-708
PAX7 (GFP) / Myogenin / Hoechst
J
Mimic-Ctr
Mimic-708
72h
Control
Odz4 -/-
Hoechst / Myogenin
Control
Odz4 -/-
% Myogenin+ cells
#p = 4.8 x 10-5
p = 0.01
p = 0.008
Mimic-Ctr
Mimic-708

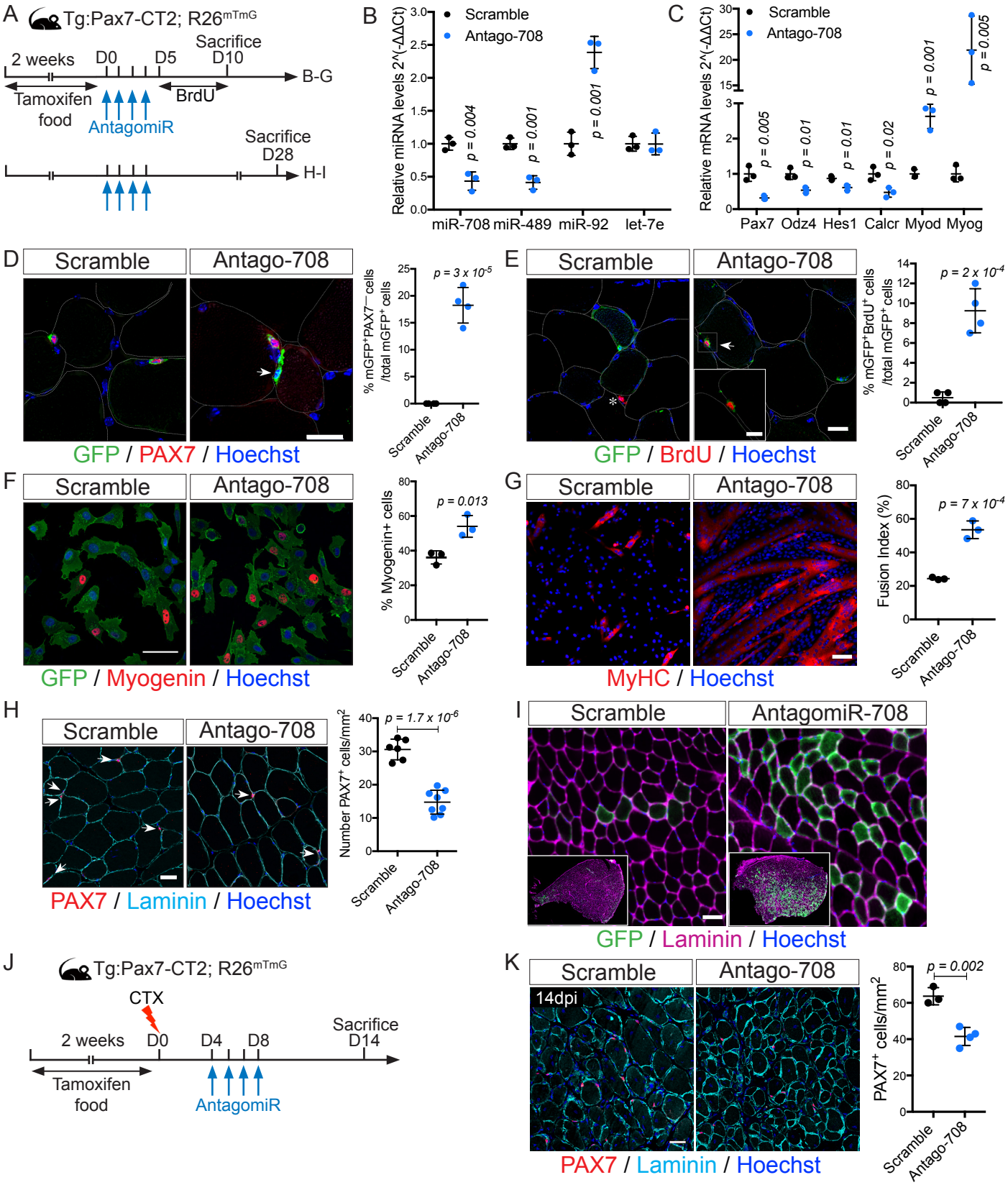
A
Tg:Pax7-CT2; R26mTmG
2 weeks
D0
D5
Sacrifice
D10
B-G
Tamoxifen
food
BrdU
AntagomiR
Sacrifice
D28
H-I
B
Scramble
Antago-708
Relative miRNA levels 2^(-ΔΔCt)
p = 0.004
p = 0.001
p = 0.001
miR-708
miR-489
miR-92
let-7e
C
Scramble
Antago-708
Relative mRNA levels 2^(-ΔΔCt)
p = 0.005
p = 0.01
p = 0.01
p = 0.02
p = 0.001
p = 0.005
Pax7
Odz4
Hes1
Calcr
Myod
Myog
D
Scramble
Antago-708
% mGFP+PAX7− cells /total mGFP+ cells
p = 3 x 10-5
GFP / PAX7 / Hoechst
E
Scramble
Antago-708
% mGFP+BrdU+ cells /total mGFP+ cells
p = 2 x 10-4
GFP / BrdU / Hoechst
F
Scramble
Antago-708
% Myogenin+ cells
p = 0.013
GFP / Myogenin / Hoechst
G
Scramble
Antago-708
Fusion Index (%)
p = 7 x 10-4
MyHC / Hoechst
H
Scramble
Antago-708
Number PAX7+ cells/mm2
p = 1.7 x 10-6
PAX7 / Laminin / Hoechst
I
Scramble
AntagomiR-708
GFP / Laminin / Hoechst
J
Tg:Pax7-CT2; R26mTmG
CTX
2 weeks
D0
D4
D8
Sacrifice
D14
Tamoxifen
food
AntagomiR
K
Scramble
Antago-708
14dpi
PAX7+ cells/mm2
p = 0.002
PAX7 / Laminin / Hoechst

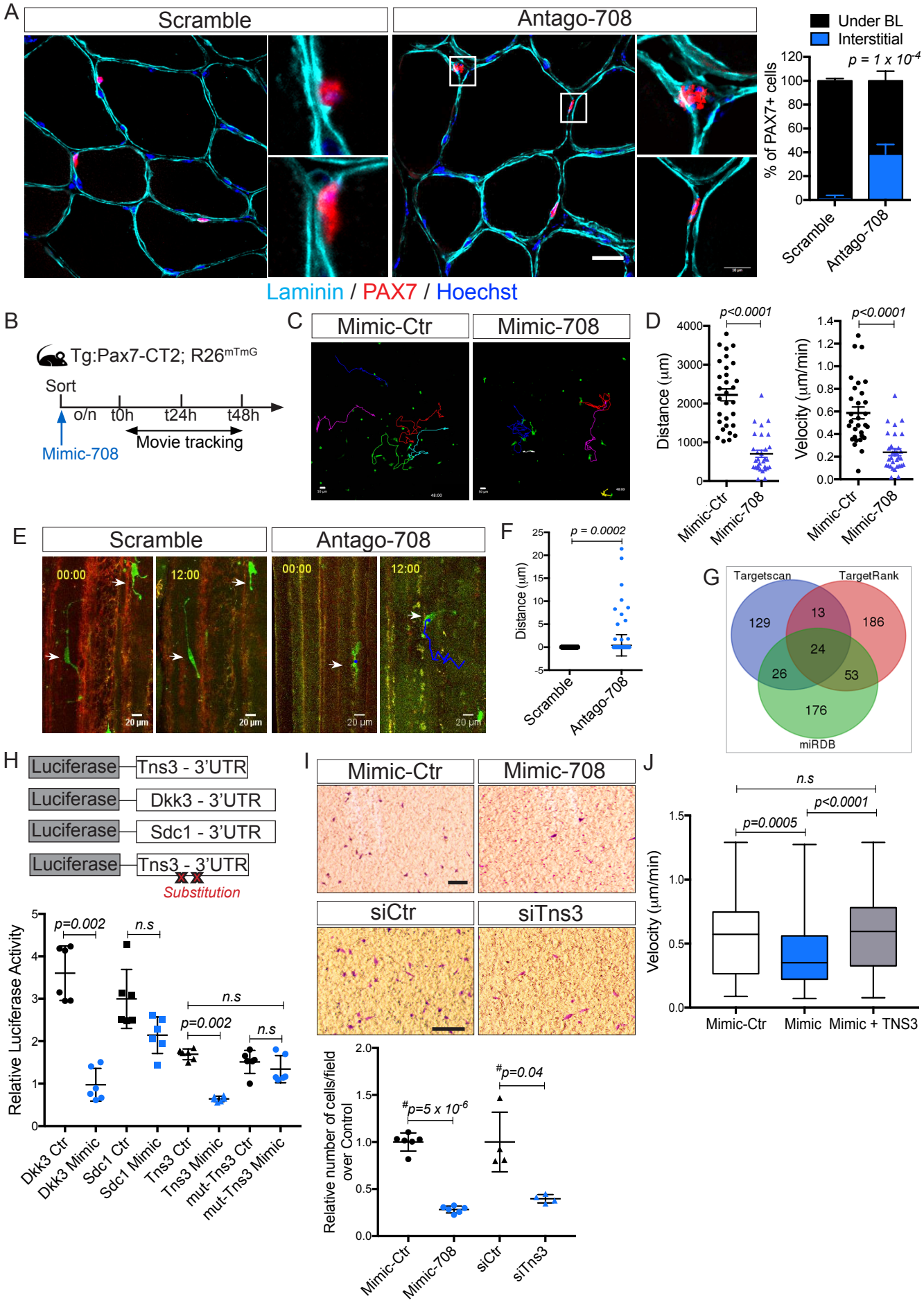
A
Scramble
Antago-708
Under BL
Interstitial
p = 1 x 10-4
% of PAX7+ cells
Scramble
Antago-708
Laminin / PAX7 / Hoechst
B
Tg:Pax7-CT2; R26mTmG
Sort
o/n
t0h
t24h
t48h
Movie tracking
Mimic-708
C
Mimic-Ctr
Mimic-708
D
p<0.0001
Distance (µm)
Velocity (µm/min)
Mimic-Ctr
Mimic-708
E
Scramble
Antago-708
00:00
12:00
20 µm
F
p = 0.0002
Distance (µm)
Scramble
Antago-708
G
Targetscan
TargetRank
miRDB
129
13
186
24
26
53
176
H
Luciferase
Tns3 - 3'UTR
Dkk3 - 3'UTR
Sdc1 - 3'UTR
Substitution
Relative Luciferase Activity
p=0.002
n.s
p=0.002
Dkk3 Ctr
Dkk3 Mimic
Sdc1 Ctr
Sdc1 Mimic
Tns3 Ctr
Tns3 Mimic
mut-Tns3 Ctr
mut-Tns3 Mimic
I
Mimic-Ctr
Mimic-708
siCtr
siTns3
Relative number of cells/field over Control
#p=5 x 10-6
#p=0.04
J
n.s
p<0.0001
p=0.0005
Velocity (µm/min)
Mimic-Ctr
Mimic
Mimic + TNS3

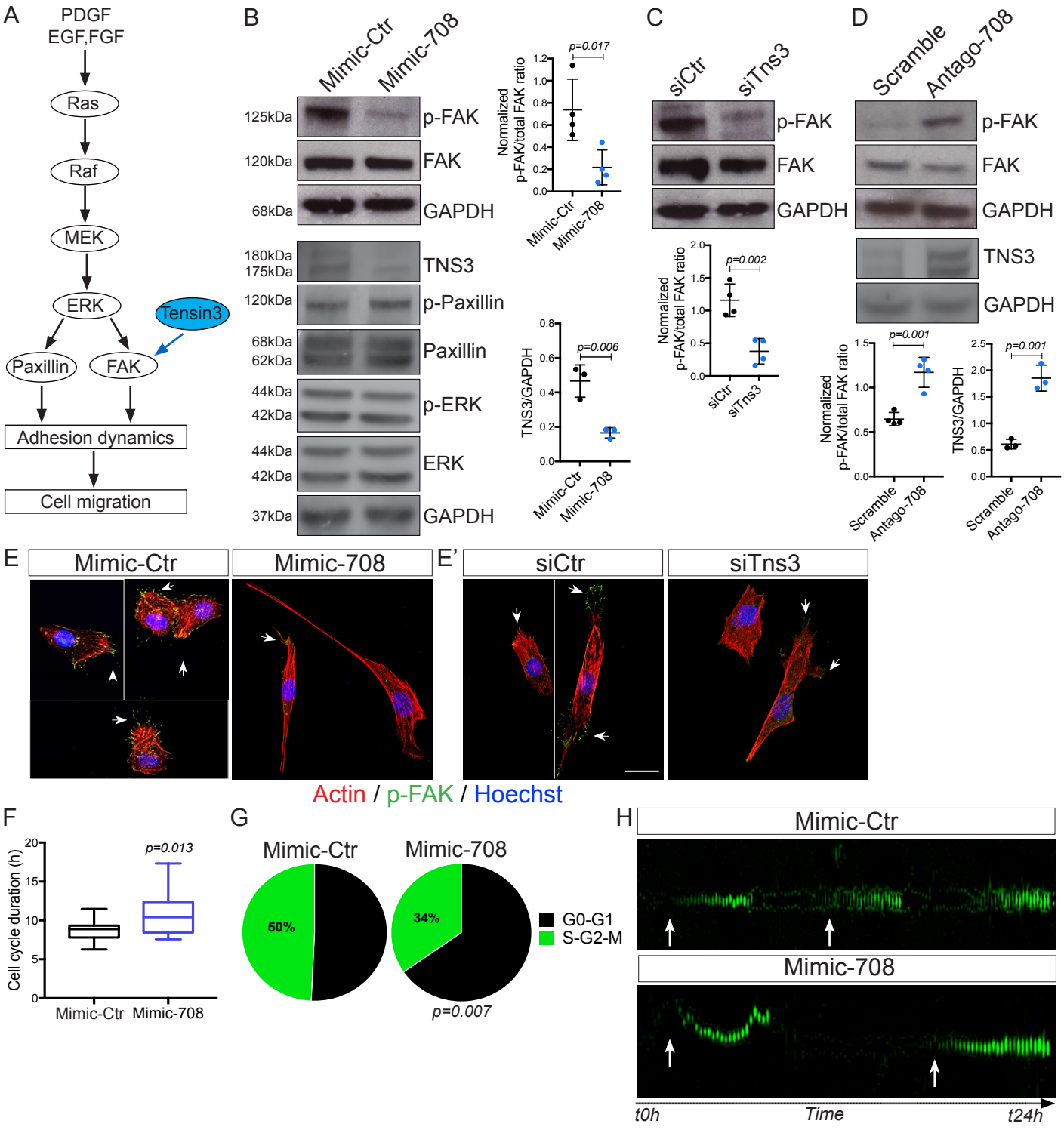
A
PDGF
EGF,FGF
Ras
Raf
MEK
ERK
Tensin3
Paxillin
FAK
Adhesion dynamics
Cell migration
B
Mimic-Ctr
Mimic-708
125kDa
p-FAK
120kDa
FAK
68kDa
GAPDH
180kDa
175kDa
TNS3
120kDa
p-Paxillin
68kDa
62kDa
Paxillin
44kDa
42kDa
p-ERK
44kDa
42kDa
ERK
37kDa
GAPDH
Normalized p-FAK/total FAK ratio
p=0.017
TNS3/GAPDH
p=0.006
C
siCtr
siTns3
p-FAK
FAK
GAPDH
Normalized p-FAK/total FAK ratio
p=0.002
D
Scramble
Antago-708
p-FAK
FAK
GAPDH
TNS3
GAPDH
Normalized p-FAK/total FAK ratio
p=0.001
TNS3/GAPDH
p=0.001
E
Mimic-Ctr
Mimic-708
E'
siCtr
siTns3
Actin / p-FAK / Hoechst
F
Cell cycle duration (h)
p=0.013
Mimic-Ctr
Mimic-708
G
Mimic-Ctr
Mimic-708
50%
34%
G0-G1
S-G2-M
p=0.007
H
Mimic-Ctr
Mimic-708
t0h
Time
t24h

Supplementary Tables related to STAR Methods

Table S1: RT-qPCR primers used in this study. Related to STAR Methods.

Mouse RT-PCR primer	Sequence (5' > 3')
Odz4_F	GTGGGATGGAGGTTAGCTCG
Odz4_R	ATGGGTTCTACTGCCCAAGTG
Hey1_F	CACCTGAAAATGCTGCACAC
Hey1_R	ATGCTCAGATAACGGGCAAC
HeyL_F	GTCTTGCAGATGACCGTGGA
HeyL_R	CTCGGGCATCAAAGAACCCT
Myod_F	CACTACAGTGGCGACTCAGATGCA
Myod_R	CCTGGACTCGCGCGCCGCCTCACT
Myogenin_F	GTGAATGCAACTCCCACAGC
Myogenin_R	CGCGAGCAAATGATCTCCTG
Pax7_F	GACAAAGGGAACCGTCTGGAT
Pax7_R	TATCTTGTGGCGGATGTGGTTA
Col4a2_F	GATACCCGGCGTAATCTCAA
Col4a2_R	ATGAGCACCTTGGAATCCTG
Rpl13_R	GTGGTCCCTGCTGCTCTCAAG
Rpl13_F	CGATAGTGCATCTTGGCCTTTT
Tbp_F	ATCCCAAGCGATTTGCTG
Tbp_R	CCTGTGCACACCATTTTTCC
Odz4 KO_F	TGAAGGAGAGGAAGCCCTATCG
Odz4 KO_R	TCACAAAGAAGCCGTCGTAGCC

Table S2: 3'-UTR of miR-708 predicted target genes. In bold: miR-708 seed sequence. Related to STAR Methods

Gene	3'UTR sequence
Dickkopf-3 (Dkk3)	GCCCAGACCCAGCTGAGTCACTGGTAGATGTGCAATAGAAATGGCTAATTTAT TTTCCCAGGAGTGTCCCCAAGTGTGGAATGGCCGCAGCTCCTTCCCAGTAGCT TTTCCTCTGGCTTGACAAGGTACAGTGCAGTACATTTCTTCCAGCCGCCCTGCT TCTCTGACTTGGGAAAGACAGGCATGGCGGGTAAGGGCAGCGGTGAGTCGTC CCTCGCTGTTGCTAGAAACGCTGTCTTGTTCTTCATGGATGGAAGATTTGTTTG AAGGGAGAGGATGGGAAGGGGTGAAGTCTGCTCATGATGGATTTGGGGGATA CAGGGAGGAGGATGCCTGCCTTGCAGACGTGGACTTGGCAAAATGTAACCTTT GCTTTTGTCTTGCGCCGCTCCCATGGGCTGAGGCAGTGGCTACACAAGAGCTA TGCTGCTCTGTGGCCTCCCACATATTCATCCCTGTGTTTC**AGCTCCTA**CCTCAC TGTCAGCACAGCCCTTCATAGCCACGCCCCCTCTTGCTCACCACAGCCTAGGA GGGGACCAGAGGGGACTTCTCTCAGAGCCCCATGCTCTCTCTCTCAACCCCAT ACCAGCCTCTGTGCCAGCGACAGTCCTTCCAAATGGAGGGAGTGAAATCCTTT GGTTTTATTATTTTCTCCTTCAAGGCACGCCTGCCACTAAGGTCAGGCTGACTT GCATGTCCCTCTAACGTTCGTAGCAGTGTGGTGGACACTGTCTTCCACCGACTG CTTCAATACCTCTGAAAGCCAGTGCTCGGAGTGCAGTTCGTGTAAATTAATTT GCAGGAAGTATACTTGGCTAATTGTAGGGCTAGGATTGTGAATGAAATTTGCA AAGTCGCTTAGCAACAATGGAAAGCCTTTCTCAGTCACACCGAGAAGTCACAA CCAAGCCAGGTTGTGTAGAGTACAGCTGTGACATACAGACAGAAGAAGGCTG GGCTGGATGTCAGGCCTCAGATGACGGTTTCAGGTGCCAGGAACTATTACCAT TCTGTATCTATCCAGAGTTATTAAAATTGAAAGTTGCACACATTTGTATAAGCA TGCCTTTCTCCTGAGTTTTAAATTATATGTATACACAAACATGTGGCCCTCAAA GATCATGCACAAACCACTACTCTTTGCTAATTCTTGGACTTTTCTCTTTGATTTT CAATAAATACAAATCCCCTTCATGCAAAAAAATTAAAACAATCTGTAGTATAA AGAGACAAAAAAATTCCATAGAAGCAGATTTTCCAGGCATCTGCAGTTTCCCT CTTTTAGAATCGGAATTCGTTGGAACTCTCATCCTTGTCTGGATGGGAATTAGC TTTAACAGAGAAACTACTTCACCCTCTCCTGAAAGAACAAATGGAATATATGA GTCTTCTCTTGGAGGCTCTTTCCACTCAAATGCAGTTCTGGGGCTGTGCTAGCA TTGATACTGTAACAAAACGGCTGAAGCAATGAACTTATATATTTAAAAAGTTA GGTTAATTGGGTTCACCATTTCAGGTTTCAGTCCTGATCCCATGGGGTTGAAAC TAAGGAGAGGCAGCACAGCGTGGCAAGGGAATGTGGTAGAGTCAAGCTGCTC CCTTTCTGGCTAACAGGAGAGTGGGCAATGTGCAGTCTTGTGAGAATGCCCAG GTCCTGGGGGGAAGGGAGTGCCCTGGACATCACCTTAAAGGTGGAGACTTCTG CAGCTTTGGTTTTAGTTACTCTTCTGGGTGCTACAATCAAACGCCCAACAAGA AGCCACCTGAGGGATGAGGGTTTATTTTGGCTCCTGGTTCAAGCAGGGAGTCC TTCGTGGCAGGAGTGCAAGGTTGCTTCCTGCAGTGTGGAGGATCAGGAAGCAA AGAAAGAGCAATGCAAGACTCAGCTTTCTCTCTTTCCCTGATTATTTATTCTGG AACCCCAACCCTTGGGGTGGTGCCGACCGCAGTAAGAGTGAGTGTCCTTTCCT TAGAACCCTCTGAAAACTCTTGGCCTCATAGAAATGTGCAGAGGTGTGTCACC TAAATTGTTCAAATCCATTCTGTTCCAAGACATGGGAGCGCTATGTGCTAAGT CTTCCACATAAGAGCACCGAGTACCTCTTAAACGCCTGTAAATCGCATCTGAA GATACCACAGTAAAGAGATGTAAACATTTAGGAAAACAATAAATGTAACTGA TGAAGTCACC
Syndecan-1 (Sdc1)	TGGGGAAATAGTTCTTTCTCCCCCCACAGCCCCTGCCACTCACTAGGCTCCCAC TTGCCTCTTCTGTGAAAAACTTCAAGCCCTGGCCTCCCCACCACTGGGTCATGT CCTCTGCACCCAGGCCCTTCCAGCTGTTCCTGCCCGAGCGGTCCCAGGGTGTG CTGGGAACTGATTCCCCTCCTTTGACTTCTGCCTAGAAGCTTGGGTGCAAAGG GTTTCTTGCATCTGATCTTTCTACCACAACCACACCTGTCGTCCACTCTTCTGA CTTGGTTTCTCCAAATGGGAGGAGACCCAGCTCTGGACAGAAAGGGGACCCG ACTGCTTTGGACCTAGATGGCCTATTGCGGCTGGAGGATCCTGAGGACAGGAG AGGGGCTTCGGCTGACCAGCCATAGCACTTACCCATAGAGACCGCTAGGGTTG GCCGTGCTGTGGTGGGGGATGGAGGCCTGAGCTCCTTGGAATCCACTTTTCAT TGTGGGGAGGTCTACTTTAGACAACTTGGTTTTGCACATATTTTCTCTAATTTC TCTGTTCAGAGCCCCAGCAGACCTTATTACTGGGGTAAGGCAAGTCTGTTGAC TGGTGTCCCTCACCTCGCTTCCCTAATCTACATTCAGGAGACCGAATCGGGGG TTAATAAGACTTTTTTTGTTTTTTGTTTTTGTTTTTAACCTAGAAGAACCAAATC TGGACGCCAAAACGTAGGCTTAGTTTGTGTGTTGTCTCTGAGTTTGTCGCTCAT

	AAGTAGGCTGGCTAGTCCAGGATACTGTGGAATAGCCACCTCTTGACCAGTCA TGCCTGTGTGCATGGACTCAGGGCCACGGCCTTGGCCTGGGCCACCGTGACAT TGGAAGAGCCTGTGTGAGAACTTACTCGAAGTTCACAGTCTAGGAGTGGAGG GGAGGAGACTGTAGAGTTTTGGGGGAGGGGTGGCAAGGGTGCCCAAGCGTCT CCCACCTTTGGTACCATCTCTAGTCATCCTTCCTCCCGGAAGTTGACAAGACAC ATCTTGAGTATGGCTGGCACTGGTTCCTCCATCAAGAACCAAGTTCACCTT**CA** **GCTCCT**GTGGCCCCGCCCCCAGGCTGGAGTCAGAAATGTTTCCCAAAGAGTG AGTCTTTTGCTTTTGGCAAAACGCTACTTAATCCAATGGGTTCTGTACAGTAGA TTTTGCAGATGTAATAAACTTTAATATAAAGGAGTCCTATGAACTCTACTGCTT CTGCTTCTTCTTCTCTGGACTGGTGGTATAGATATAGCCACCCTTTGCCCAAAC CCTGGTAGCTCGGGGAAGCTTGGCTTAAGGCTGCACGCCTCCAATCCCCCAAA GGGTAGGATCCTGGCTGGGTCCAGGGTTCCTCTGATTTATTTGGTTTTGTTGTG TTGTGTTGTGTTTTTCTTTTGGCTAAACTTCTTTTGGAAGTTGGTAAGTTCAGCC AAGGTTTTACAGGCCCTGATGTCTGTTCTTCTAAATGGTTTAAGTAATTGGGAC TCTAGCACATCTTGACCTAGGGTCACTAGAGCTAAGCTTGCTTTGCAGGGCAG ACACCTGGGACAGCCTTCCTCCCTCATGTTTGCTGGGACACTGCTGAGCACCC CTTGCTTACTTAGCTCAGTGATGTTCCAGCTCCTGGCTAGGCTGCTCAGCCACT CAGCTAGACAAAAGATCTGTGCCCTGTGTTTCATCCCAGAGCTTGTTGCCAGA TCACATGGCTGGATGTGATGTGGGGTGGGGGTGGGGTCATATCTGAGACAGCC CTCAGCTGAGGGCTTGTGGGACAGTGTCCAAGCCTCAGGCTGGGCTCATTCAT ATAATTGCAATAA
Tensin-3 **(Tns3)**	GTCTGTGTGTATACAGGTGGACCATTCCACTTTATGCTCATGTATGTCTGTGTG TATACAGGTGGACCATTCCACTTTTGCTCATGTATGTCTGTGTGTATACAGGTG GACTATTCCACTTTTT**AGCTCCTA**TTGATGCACCAAAAGCAAGTGCCTCATTT CTGTGCCAAATGTTTGCCTTGGTCTTTAAGGACCTCCTTCGTGGACACTCTGAT GTGCCTGTTAGAGGGAATGTGCCACCATTCCCTAGAGGCCCCATGTCTTCCAC AGAGGCTTCTAGTGTTCCAGTTACTCATATGCAGCTAAACTCCAGATGGGGGC AGGGGTGGGGCTGAAGTTGTGCTCTAAGAAGTATCACATCCTATGATTATAAG TTTATATGCAGATGTGGCCCAGAGATCACAGCCCCGCACTCTTTTCCTCCCGCT GGAGGGGGGTGGGGGTGGGGGGAGAGGGCCTAATTAGAAACTCAGCTGGGCT CTGCTGAAGCCCAGCTTTCCGGTGAATTGAATGCCCACAAAGGTTGGCATGGA ATGGCATCCAAGAAGCCACAACGAATGTGCGTTTCAAAACTGACCGGGAGGG TATGATTCTTACTCCAGGATACAAGTCAGTCCAGGGTATCCAGGATCGACTGA GGGAACCCAGGGAGACCGTCCACATGGTACAAACACTGGGGGCGGCCGGAAC GAGGGAAGCGGGTTGACAACACAACGGACTACACACCGGGGCCCACACGGAC GAATACACAGT
Mutated **Tensin-3**	GTCTGTGTGTATACAGGTGGACCATTCCACTTTATGCTCATGTATGTCTGTGTG TATACAGGTGGACCATTCCACTTTTGCTCATGTATGTCTGTGTGTATACAGGTG GACTATTCCACTTTTT**AGC<u>GAA</u>TA**TTGATGCACCAAAAGCAAGTGCCTCATTT CTGTGCCAAATGTTTGCCTTGGTCTTTAAGGACCTCCTTCGTGGACACTCTGAT GTGCCTGTTAGAGGGAATGTGCCACCATTCCCTAGAGGCCCCATGTCTTCCAC AGAGGCTTCTAGTGTTCCAGTTACTCATATGCAGCTAAACTCCAGATGGGGGC AGGGGTGGGGCTGAAGTTGTGCTCTAAGAAGTATCACATCCTATGATTATAAG TTTATATGCAGATGTGGCCCAGAGATCACAGCCCCGCACTCTTTTCCTCCCGCT GGAGGGGGGTGGGGGTGGGGGGAGAGGGCCTAATTAGAAACTCAGCTGGGCT CTGCTGAAGCCCAGCTTTCCGGTGAATTGAATGCCCACAAAGGTTGGCATGGA ATGGCATCCAAGAAGCCACAACGAATGTGCGTTTCAAAACTGACCGGGAGGG TATGATTCTTACTCCAGGATACAAGTCAGTCCAGGGTATCCAGGATCGACTGA GGGAACCCAGGGAGACCGTCCACATGGTACAAACACTGGGGGCGGCCGGAAC GAGGGAAGCGGGTTGACAACACAACGGACTACACACCGGGGCCCACACGGAC GAATACACAGT

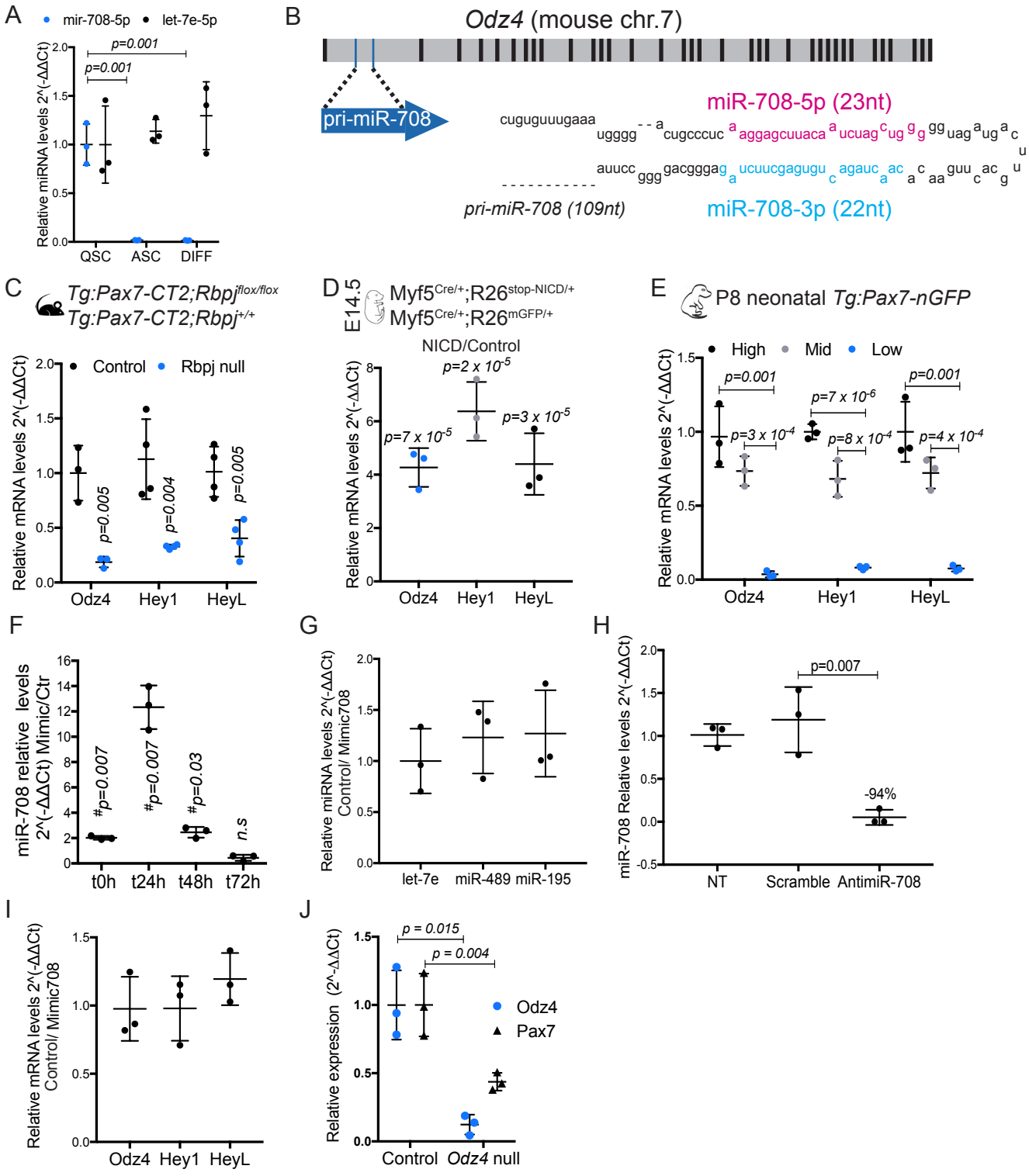
A
mir-708-5p
let-7e-5p
p=0.001
p=0.001
Relative miRNA levels 2^(-ΔΔCt)
QSC
ASC
DIFF
B
Odz4 (mouse chr.7)
pri-miR-708
miR-708-5p (23nt)
miR-708-3p (22nt)
pri-miR-708 (109nt)
C
Tg:Pax7-CT2;Rbpj flox/flox
Tg:Pax7-CT2;Rbpj +/+
Control
Rbpj null
p=0.005
p=0.004
p=0.005
Odz4
Hey1
HeyL
D
E14.5
Myf5 Cre/+;R26 stop-NICD/+
Myf5 Cre/+;R26 mGFP/+
NICD/Control
p=7 x 10-5
p=2 x 10-5
p=3 x 10-5
E
P8 neonatal Tg:Pax7-nGFP
High
Mid
Low
p=0.001
p=3 x 10-4
p=7 x 10-6
p=8 x 10-4
p=0.001
p=4 x 10-4
F
miR-708 relative levels 2^(-ΔΔCt) Mimic/Ctr
#p=0.007
#p=0.007
#p=0.03
n.s
t0h
t24h
t48h
t72h
G
Relative miRNA levels 2^(-ΔΔCt) Control/ Mimic708
let-7e
miR-489
miR-195
H
miR-708 Relative levels 2^(-ΔΔCt)
p=0.007
-94%
NT
Scramble
AntimiR-708
I
Relative mRNA levels 2^(-ΔΔCt) Control/ Mimic708
Odz4
Hey1
HeyL
J
Relative expression (2^-ΔΔCt)
p = 0.015
p = 0.004
Odz4
Pax7
Control
Odz4 null

Fig. S1 related to Fig.1. Assessment of miR-708 expression in subpopulations of satellite cells and *ex vivo* gain and loss of function validations.

(A) RT-qPCR validation of miR-708 expression on freshly isolated satellite cells (QSC), *in vivo* activated (ASC) satellite cells at 5 days post-injury of *Tibialis anterior* (TA) muscle, and freshly isolated myofibres from *Extensor digitorum longus* (EDL) muscle (DIFF). Let-7e expression was stable in every condition (see Fig. 1A) and was used as a negative control; (n=3 mice/condition).

(B) Scheme of mouse *Odz4* gene; black boxes represent exons. miR-708 is encoded by the first intron of *Odz4*. Stem loop sequence of pri-miR-708 (109 nt) including miR-708-5p (pink; aaggagcuuacaaucuagcuggg), the mature strand in satellite cells and the passenger strand, miR-708-3p (blue; caacuagacugugagcuucuag). The miR-708-5p strand constitutes the major mature form of miR-708 in satellite cells, while the passenger strand miR-708-3p was in minority. Therefore, we focused on miR-708-5p (Accession MIMAT0004828) for the remaining experiments in this study.

(C) RT-qPCR analysis of *Odz4* gene in *Rbpj* conditional KO (*Rbpj* null) and Control satellite cells. Cells were isolated from resting muscles by FACS 2-weeks post-tamoxifen treatment. Control: *Tg:Pax7-CT2; Rbpj*$^{+/+}$*; R26*^{mTmG} and *Rbpj* null: *Tg:Pax7-CT2; Rbpj*$^{flox/flox}$*; R26*^{mTmG}; n=4 mice/genotype.

(D) Induction of *Odz4* gene in E14.5 control (*Myf5*$^{Cre/+}$*; R26*$^{mTmG/+}$) and *Myf5*^{Cre}*-NICD* (*Myf5*$^{Cre/+}$*; R26*$^{stop\text{-}NICD\text{-}nGFP/+}$) myogenic cells isolated by FACS assessed by RT-qPCR. *Hey1 and HeyL* are reporters of Notch activity; n=4 fetuses/genotype.

(E) Transcript expression levels of *Odz4* targeted by Notch in cells fractionated by FACS based on GFP-intensity from *Tg:Pax7-nGFP* at postnatal day 8 (P8) where Notch activity gradually decreases from the more committed (high) to more differentiated (low) cells: Pax7^{High} 20% of population (black), Pax7^{Mid} 40% (grey) and Pax7^{Low} 20% (blue); n=3 pups.

(F) RT-qPCR of miR-708 expression at 4h, 24h, 48h and 72h after Mimic-708 transfection of satellite cells isolated from adult *Tg:Pax7-nGFP* mice; n=3 mice.

(G) RT-qPCR of quiescent-specific miRNAs, miR-489 and miR-195, showing that miR-708 overexpression is specific to a single miRNA; n=3 mice.

(H) Transcript levels of miR-708 in satellite cells isolated from *Tg:Pax7-nGFP* at 12h after miR-708 inhibition using AntimiR-708 transfection; n=3 mice.

(I) Transcripts levels of Odz4 following miR-708 overexpression (24h post-transfection).

(J) RT-qPCR of *Odz4* and *Pax7* in Control and knock-out (*Odz4* KO) mice. Note that *Pax7* is downregulated in *Odz4* KO satellite cells; n=3 mice/genotype.

Error bars, mean ± SD; two-sided unpaired t-test; $^{\#}$p-value: two-sided paired t-test.

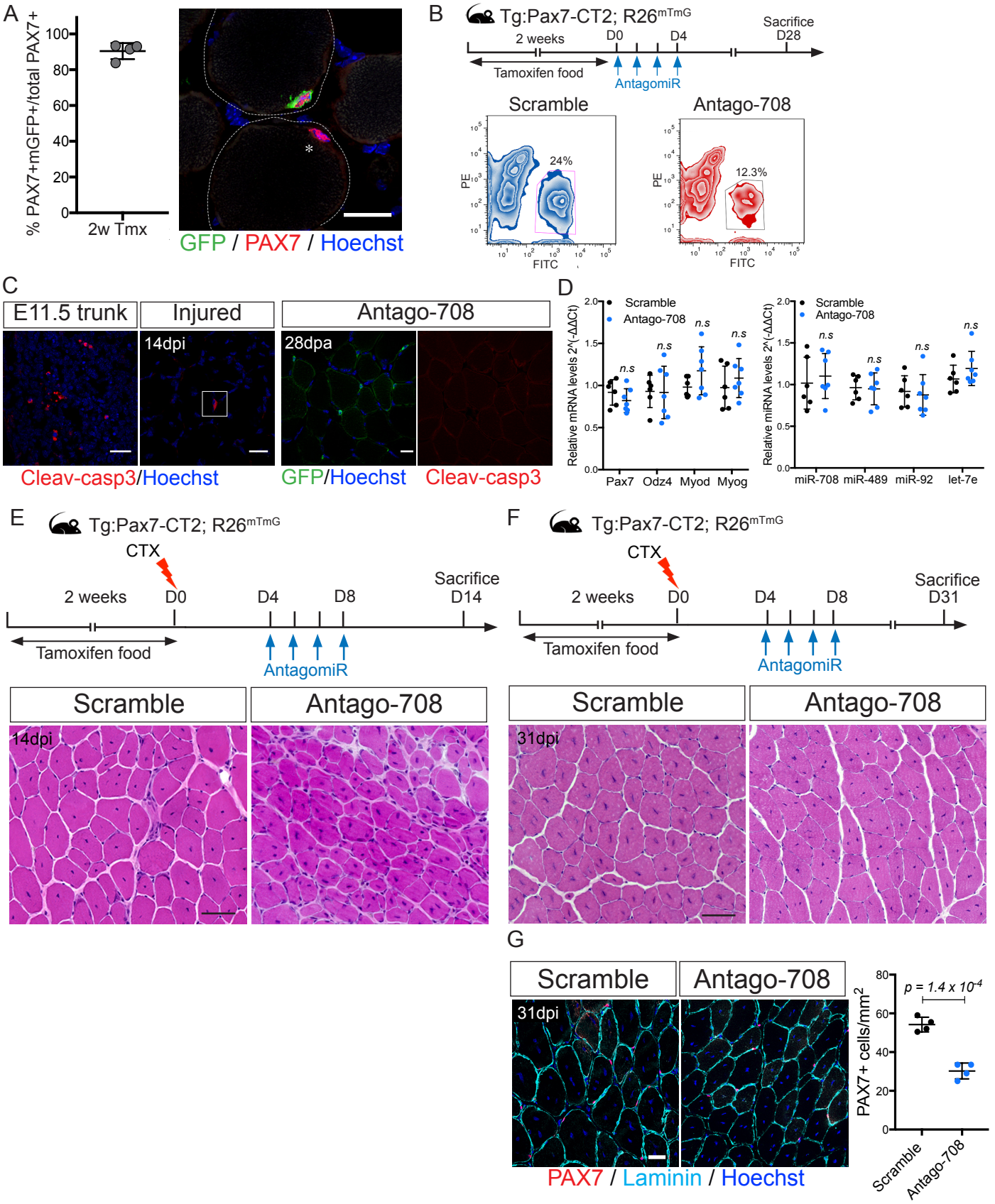
A
% PAX7+mGFP+/total PAX7+
100
80
60
40
20
0
2w Tmx
GFP / PAX7 / Hoechst
B
Tg:Pax7-CT2; R26mTmG
2 weeks
D0
D4
Sacrifice
D28
Tamoxifen food
AntagomiR
Scramble
Antago-708
24%
12.3%
PE
FITC
C
E11.5 trunk
Injured
Antago-708
14dpi
28dpa
Cleav-casp3/Hoechst
GFP/Hoechst
Cleav-casp3
D
Scramble
Antago-708
Relative mRNA levels 2^(-ΔΔCt)
n.s
Pax7
Odz4
Myod
Myog
Relative miRNA levels 2^(-ΔΔCt)
miR-708
miR-489
miR-92
let-7e
E
Tg:Pax7-CT2; R26mTmG
CTX
2 weeks
D0
D4
D8
Sacrifice
D14
Tamoxifen food
AntagomiR
Scramble
Antago-708
14dpi
F
Tg:Pax7-CT2; R26mTmG
CTX
2 weeks
D0
D4
D8
Sacrifice
D31
Tamoxifen food
AntagomiR
Scramble
Antago-708
31dpi
G
Scramble
Antago-708
31dpi
PAX7 / Laminin / Hoechst
PAX7+ cells/mm2
p = 1.4 x 10-4
Scramble
Antago-708

Fig. S2 related to Fig.2. *In vivo* inhibition of miR-708 induces spontaneous differentiation.

(A) Recombination efficiency of *Tg:Pax7-CT2; R26*^{mTmG} mice fed two weeks with tamoxifen food and assessed by quantification of mGFP+/ PAX7+ cells over total PAX7+ cells in TA sections. After two weeks of treatment, 95-97% of satellite cells (PAX7+) were recombined (mGFP+). Asterisk shows a non-recombined cell (PAX7+mGFP-); n=4 mice.

(B) Scheme of tamoxifen and AntagomiR administration to *Tg:Pax7-CT2; R26*^{mTmG} mice. AntagomiR-708 and Scramble control were injected daily for 4 days after the end of tamoxifen treatment (D0) and mice were sacrificed 28 days post-AntagomiR treatment. FACS profiles of mGFP-positive cells from resting muscles of control (Scramble) or AntagomiR-708 treated mice show decrease in satellite cell numbers 28 days after miR-708 *in vivo* inhibition.

(C) Cleaved-caspase3 immunostaining showed no apoptosis in quiescent satellite cells treated with AntagomiR-708. Sections from E11.5 trunk embryo and injured TA are shown as positive controls; n=3 mice.

(D) RT-qPCR of mGFP-positive cells isolated from resting muscle of Scramble or AntagomiR-708 treated mice after 28 days (see also Fig. S2B). Expression of quiescence (*Pax7*, *Odz4*), activation (*Myod*) and differentiation (*Myogenin*) genes was not affected (left); quiescent miR-708, miR-489 and activated miR-92 expression levels are similar in Scramble and AntagomiR-708 treated satellite cells (right); n=6 Scramble and n=7 AntagomiR treated mice.

(E)(F) Schemes of miR-708 *in vivo* knock-down. *Tg:Pax7-CT2; R26*^{mTmG} mice were fed with tamoxifen for 2 weeks. Four days following Cardiotoxin injury (CTX), AntagomiR-708, or Scramble were injected every day for 4 days and injured muscles were collected 14 days (E) or 31 days (F) post-injury. Hematoxylin and Eosin staining of transverse sections of regenerating TA muscles 14 days (E) or 31 days (F) post-injury show miR-708 *in vivo* knock down induced a delay in muscle regeneration at 14 days post injury, but histology looks similar in both conditions at 31 days post-injury; n= 4 mice/treatment.

(G) Quantification of number of satellite cells/mm^2 on TA sections from Scramble and AntagomiR-treated mice 31dpi stained with Laminin and PAX7; n=4 mice/treatment.

Error bars, mean ± SD; two-sided unpaired t-test. Scale bar 10µm (A), 50µm (C, G) and 100µm (E, F).

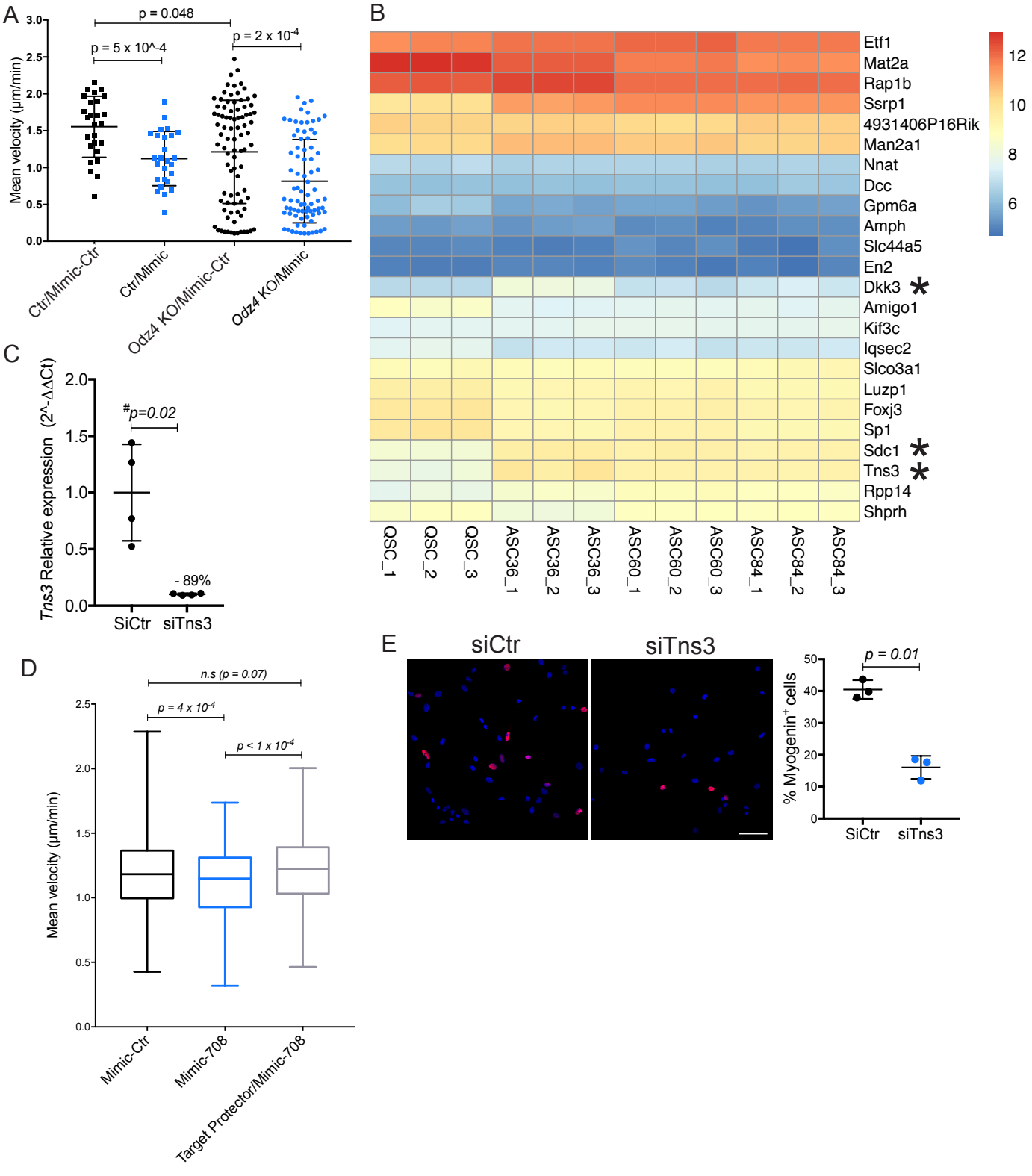
A
p = 0.048
p = 5 x 10^-4
p = 2 x 10^-4
Mean velocity (µm/min)
Ctr/Mimic-Ctr
Ctr/Mimic
Odz4 KO/Mimic-Ctr
Odz4 KO/Mimic
B
Etf1
Mat2a
Rap1b
Ssrp1
4931406P16Rik
Man2a1
Nnat
Dcc
Gpm6a
Amph
Slc44a5
En2
Dkk3 *
Amigo1
Kif3c
Iqsec2
Slco3a1
Luzp1
Foxj3
Sp1
Sdc1 *
Tns3 *
Rpp14
Shprh
QSC_1
QSC_2
QSC_3
ASC36_1
ASC36_2
ASC36_3
ASC60_1
ASC60_2
ASC60_3
ASC84_1
ASC84_2
ASC84_3
C
Tns3 Relative expression (2^-ΔΔCt)
#p=0.02
- 89%
SiCtr
siTns3
D
n.s (p = 0.07)
p = 4 x 10-4
p < 1 x 10-4
Mean velocity (µm/min)
Mimic-Ctr
Mimic-708
Target Protector/Mimic-708
E
siCtr
siTns3
p = 0.01
% Myogenin+ cells
SiCtr
siTns3

Fig. S3 related to Fig.3. miR-708 predicted target genes.

(A) Velocity of control and *Odz4*-null satellite cells overexpressing miR-708 (Mimic) or control RNA oligonucleotide (Ctr) assessed by live videomicroscopy for 32h. Note that motility in presence (control) and absence (*Odz4* KO) of *Odz4* is similar; n=3 mice/ genotype/treatment.

(B) Gene expression microarray data show 24 genes predicted by the 3 logarithms (TargetScan, TargetRank and Miranda) in satellite cells. The data are shown as a heatmap of normalized transcripts expressed in quiescence (QSC) and different time points post injury (36h (ASC36), 60h (ASC60) and 84h (ASC84); GEO accession number GSE52192 (Liu et al., 2013)). Note that only *Dkk3*, *Tns3* and *Sdc1* were upregulated during activation. Asterisks show genes of interest.

(C) Efficiency of knock-down shown by RT-qPCR on C2C12 cells transfected with siTns3 and siRNA control; n= 4 independent experiments.

(D) Target Protector Assay (where Tns3 3'UTR is occupied by a morpholino masking miR-708 binding site; see Methods) on satellite cells isolated from *Tg:Pax7-nGFP*, imaged and tracked for 8h upon transfection; n≤200 cells tracked from 2 independent experiments.

(**E)** Knock-down of *Tns3* (siTns3) on freshly isolated satellite cells from *Tg:Pax7-nGFP* mice decreased differentiation at 72h of culture; n=3 mice/condition.

Error bars, mean ± SD; Mann-Whitney test (A, D), two-sided paired (C), unpaired t-test (E). Scale bar: 50μm.

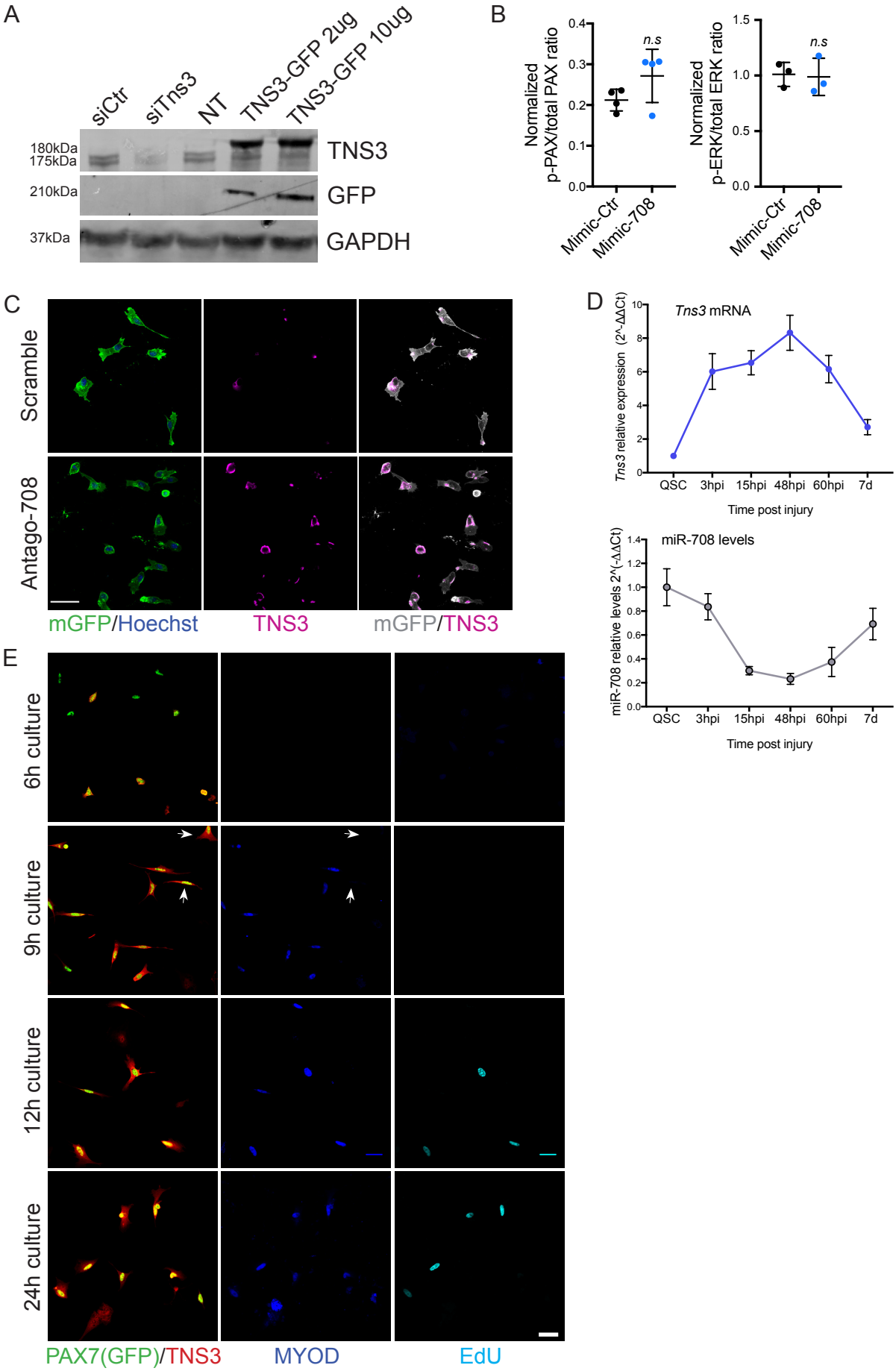
A
siCtr
siTns3
NT
TNS3-GFP 2ug
TNS3-GFP 10ug
180kDa
175kDa
TNS3
210kDa
GFP
37kDa
GAPDH
B
Normalized p-PAX/total PAX ratio
n.s
Mimic-Ctr
Mimic-708
Normalized p-ERK/total ERK ratio
n.s
Mimic-Ctr
Mimic-708
C
Scramble
Antago-708
mGFP/Hoechst
TNS3
mGFP/TNS3
D
Tns3 mRNA
Tns3 relative expression (2^-ΔΔCt)
QSC
3hpi
15hpi
48hpi
60hpi
7d
Time post injury
miR-708 levels
miR-708 relative levels 2^(-ΔΔCt)
QSC
3hpi
15hpi
48hpi
60hpi
7d
Time post injury
E
6h culture
9h culture
12h culture
24h culture
PAX7(GFP)/TNS3
MYOD
EdU

Fig. S4 related to Fig.4. miR-708 targets Tns3 to release cell migration and promote activation.

(A) Validation of Tns3 (see Table 2) antibody by knock-down of *Tns3* (siTns3) in C2C12 myoblasts 48h after siRNA transfection. Scramble siRNA and non-transfected (NT) cells were used as negative controls; overexpression of TNS3-GFP expressing plasmid served as positive control. Two specific bands about 175 and 180kDa in size correspond to TNS3, the higher one likely resulting from post-translational modification. Note that both bands are decreased upon *Tns3* knock-down.

(B) Quantification of ERK and Paxillin phosphorylation state upon miR-708 induction compared to control in C2C12 myoblasts. Western-blots were normalized to GAPDH levels; n=3-4 independent experiments. Error bars, mean ± SD; two-sided unpaired t-test.

(C) Immunostaining of TNS3 and mGFP on satellite cells isolated by FACS from Scramble and AntagomiR-708 treated mice (10d post treatment) plated for 12h before fixation. TNS3 is strongly upregulated when miR-708 is repressed (see Fig. 4D).

(D) Time course of *Tns3* and miR-708 expression performed by RT-qPCR on freshly isolated satellite cells (QSC), 3h, 15h, 48h, 60h or 7 days after Cardiotoxin injury of TA muscle of *Tg:Pax7-nGFP* mice; n=4 mice/condition.

(E) Representative images of PAX7-nGFP+ satellite cells from total muscle preparations plated for indicated times and stained for EdU (2h pulse), GFP, TNS3, and MYOD. At 6h, no MYOD+ or EdU+ cells were detected. At 9h, arrows point TNS3+/MYOD- cells. Scale bar 25µm.